

Geophysical electromagnetic modeling and evaluation: a review

Bochen Wang^{1,2,3}, Jianxin Liu^{1,2,3}, Xiangping Hu⁴, Jiawei Liu^{1,2,3}, Zhenwei Guo^{1,2,3*},
Jianping Xiao^{1,2,3}

- 1 School of Geosciences and Info-physics, Central South University, Changsha, 410083, China;
2 Hunan Key Laboratory of Nonferrous Resources and Geological Hazard Exploration,
3 Changsha 410083, China;
4 Key Laboratory of Metallogenic Prediction of Nonferrous Metals and Geological Environment
5 Monitoring (Central South University), Ministry of Education, Changsha 410083, China;
6 bochenwang29@csu.edu.cn; ljsx6666@126.com; jw-liu@csu.edu.cn; guozhenwei@csu.edu.cn;
7 jpxiao@csu.edu.cn;
8 4 Department of Energy and Process Engineering, Norwegian University of Science and
9 Technology, 7491, Trondheim, Norway; xiangping.hu@ntnu.no;

*Corresponding author: guozhenwei@csu.edu.cn

Abstract

Electromagnetic forward modeling is the cornerstone of geophysical electromagnetic inversion. During the last 50 years, numerical simulation methods have been rapidly developed and widely used in geophysical area as the computational capacity continued to increase, such as from single-core to the most modern multi-core processing cards. This paper reviews the literature of electromagnetic fields simulation, particularly focusing on the forward modeling methods include finite difference method, finite element method, integral equation method, and several hybrid methods. We also discuss the possibility of deep learning methods for EM modeling. By sorting out the work done by the predecessors, this review briefly introduces the basic principles and traces back the development of these methods. We propose a Qualitative Evaluation Model named STAMP Model and some criteria of qualitative evaluation on these methods will be discussed in this model.

Keywords: electromagnetic modeling; finite difference method; finite element method; integral equation method

1 Introduction

Geophysical electromagnetic (EM) methods are effectively and widely applied in geophysical researches, applied geophysics and engineering. They mainly reflect the contrast of the electrical conductivity and the magnetic permeability between the targets and surrounding rocks. Accurate simulation of the EM fields distribution has become the primary goal for the EM exploration. Since it is impossible to obtain the analytical solutions of multi-dimensional Maxwell's equations in real complex medium underground, geophysicists devote to find out the numerically approximate

42 solutions for EM fields modeling. EM inversion estimates the realistic subsurface
43 electromagnetic fields distribution, which depends on the precise solution of EM
44 forward modeling problem.

45 During the past 50 years, the development of the modeling has experienced from
46 low to high dimension (generally from one-dimensional (1D) to two-dimensional
47 (2D), three-dimensional (3D) and two-and-half-dimensional (2.5D) problems), from
48 simple to complex geometry, and from isotropic to anisotropic structure. Application
49 of EM fields modeling has been used in the EM exploration with onshore, offshore,
50 airborne, and borehole environments. With the rapid development of computers and
51 numerical methods, the complexity of the problems to be solved has gradually
52 increased, which has caused a enormous calculational burden. In order to improve
53 computing efficiency, modern computer distributed platforms provide good technical
54 supports for parallel computing.

55 Geophysical EM forward modeling is sometimes regarded as an engine for EM
56 inversion and commonly used to obtain the verification of conductivity models or
57 conduct various related feasibility studies (Avdeev, 2005). Virieux et al. (2011)
58 mentioned that the key indicators for choosing the forward modeling method mainly
59 included the accuracy, the efficiency, the practicality of the method and the gradient of
60 the misfit function in an inversion algorithm. Researchers committed to advance the
61 forward modeling to higher accuracy and faster computational speed (Kosloff and
62 Baysal, 1982; Zhang et al., 1995; Heagy et al., 2019).

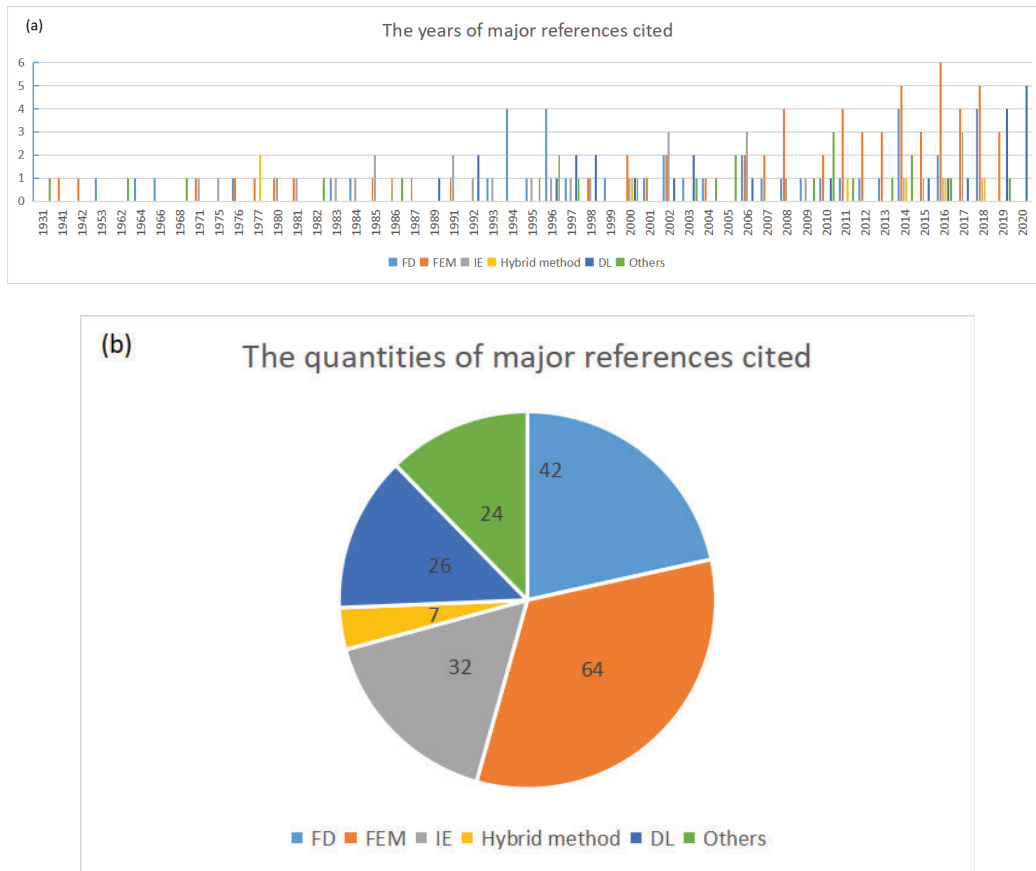
63 There are some review articles on the EM forward modeling methods. Some
64 articles are focusing on some specific problems, such as EM applications in
65 hydrocarbon exploration and monitoring, partly mentioned the modeling problems
66 (Kaikkonen, 1986; Sheard et al., 2005; Siemon et al., 2009; Strack, 2014; Streich,
67 2016). Avdeev (2005) mentioned numerical methods from theory to application
68 focusing on the 3D problem. Zhdanov (2010) discussed the EM methods exhaustively,
69 including the developments of data acquisition, modeling, inversion and interpretation,
70 as well as a new approach to EM-field characterization. Börner (2010) considered the
71 numerical solution of the 3D time-domain and frequency-domain EM induction
72 problems, restricted to finite difference method (FD) and finite element method (FEM)
73 and consciously ignoring integral equation method (IE). From the perspective of
74 numerical calculations, Miensoopust et al. (2013) compared different algorithms from
75 the two aspects of forward and inversion methods and discussed the applicability of
76 these different algorithms to the two Dublin models. Newman (2014) reviewed high
77 performance computational (HPC) strategies for large-scale 3D EM modeling and
78 imaging and discussed the future of HPC applied to EM modeling.

79 Differently from the above reviews, in this paper we mainly review the three
80 most widely applied methods for EM modeling, including FD, FEM and IE, and
81 several hybrid methods derived from them. We will intentionally not elaborate on
82 some details of numerical calculation and parallel computing. Our aim is to catch the
83 recent development of the EM forward modeling methods. In order to give readers a
84 clearer understanding of the EM forward modeling, we stand at the point of the
85 development history and the improvement of these methods.

86 In Section 2, we first review FD, FEM, IE respectively and divide some key
 87 technologies of them more carefully according to their respective characteristics. Then
 88 we also mention several hybrid methods derived from the above three methods. The
 89 hybrid methods generally combine advantages of at least two of these conventional
 90 methods to make up for the shortcomings of single methods. Additionally, we discuss
 91 the possibility of the application of the deep learning (DL) method in EM modeling.

92 In Section 3, we discuss on the basis of the traditional EM modeling methods
 93 reviewed in the previous part and build up an evaluation model, called STAMP Model,
 94 to qualitatively describe the advantages and disadvantages of the forward modeling
 95 methods. In the last, we make a conclusion for this review paper.

96 The statistics for the years and quantities of major references cited are given in
 97 Figure 1. What we can find interesting is that after 2000, researchers began to study
 98 FEM gradually, and in the past five years, deep learning began to become the focus of
 99 researchers' attention.



100

101

102 Figure 1. The statistics for the years (a) and quantities (b) of major references cited.

1
2
3
4
5
6
7
8
9
10
11
12
13
14
15
16
17
18
19
20
21
22
23
24
25
26
27
28
29
30
31
32
33
34
35
36
37
38
39
40
41
42
43
44
45
46
47
48
49
50
51
52
53
54
55
56
57
58
59
60
61
62
63
64
65

1 103 **2. Commonly use numerical approaches**

2
3
4
5 104 **2.1 Finite difference method**

6
7
8 105 Finite difference (FD) method is an approximate numerical solution for
9 106 differential equations (DE), which discretizes the derivative in the governing
10 107 equations mainly by Taylor series expansion. With it, the algebraic equation with
11 108 unknown variables on the grid can be established and then the differential equation
12 109 system is directly turned into an algebraic problem.

13
14
15 110 Finite difference method is one of the earliest methods used in computer
16 111 numerical simulation. In the 1960s, Yee (1966) first adopted FD to solve the initial
17 112 boundary problem of time-domain Maxwell's equations in the isotropic medium, and
18 113 proposed the staggered-grid finite-difference method (SFD). According to the
19 114 different solution domain, it can be divided into finite-difference time-domain method
20 115 (FDTD) and finite-difference frequency-domain method (FDFD). SFD as the most
21 116 commonly used difference format can solve for the EM fields in both the time and
22 117 frequency domain.

23
24
25
26
27 118 **2.1.1 SFD in EM modeling**

28
29
30 119 The staggered-grid finite-difference method (SFD) is a method meshing in space.
31 120 In the conventional staggered grids (SG), the scalar is stored and calculated on the
32 121 normal grid node, and the components of the vector are stored and calculated on the
33 122 dislocated grid. The center of the dislocated grid is located on the interface of the
34 123 original control volume. And the purpose of using SG is to solve the discontinuity
35 124 problem caused by the discrete governing equations on ordinary grids. In view of this
36 125 advantage, Yee (1966) proposed SFD suitable for EM modeling.

37
38
39
40
41 126 *Yee grids*

42
43 127 Yee's SFD defines the discrete electric field components at the midpoint of the
44 128 edges of the discrete elements, while the discrete magnetic field components are
45 129 defined at the centers of each side facet of the discrete elements. The defined position
46 130 of the EM fields can be exchanged. On the one hand, Yee's SFD naturally expresses
47 131 Faraday's right-handed spiral law of electromagnetic induction. On the other hand, it
48 132 solves the problem of the discontinuity of the tangential components of the electric
49 133 field caused by the electric field definition at the nodes of the elements in the
50 134 conventional grids. Figure 2 shows the staggered grid (Yee, 1966) and the
51 135 conventional grid for the FD method on the EM modeling. Unless otherwise specified,
52 136 the "SFD" used below is Yee's SFD.
53
54
55
56
57
58
59
60
61
62
63
64
65

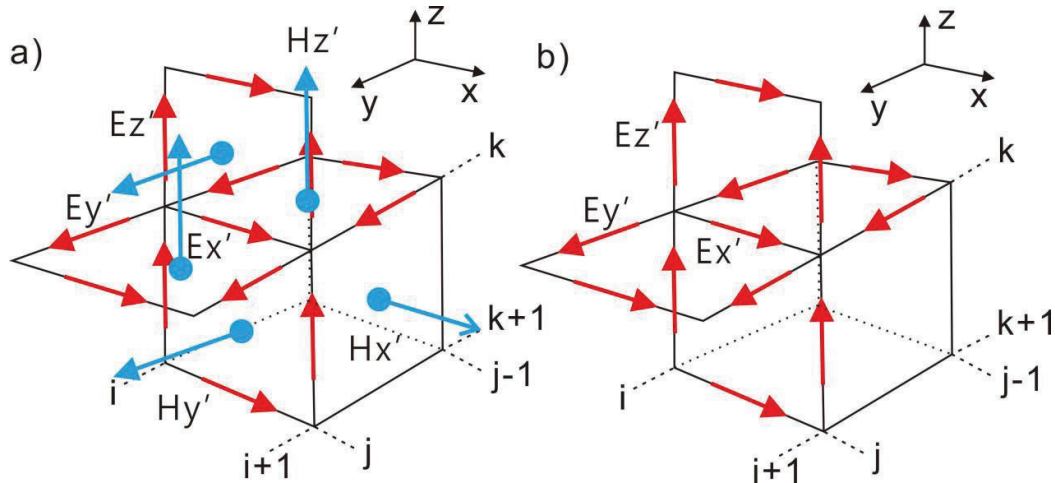


Figure 2. The staggered grid (a) and the conventional grid (b) for the FD method. The red arrows represent the electric field components E' and the blue arrows represent the magnetic field components H' (the electric field components E' and the magnetic field components H' are coincident in b). (Modified from Weiss and Newman, 2002)

Due to the limitations of computer development, the SFD algorithm was not widely used until the 1990s. Newman and Alumbaugh (1995) employed SFD method to the 3D frequency-domain AEM response and Alumbaugh et al. (1996) applied it for solving the 3D earth wideband EM response. Smith (1996a) developed the SFD for 3D electromagnetic induction directly on the inhomogeneous rectangular grid and discussed the derivation process of SFD equation. The solution was compared with the 2D quasi-analytical solution and the accuracy of the method was proved. Smith also pointed out that the various differential relationships between different field components must be completely maintained in the SFD form, which was the most important feature of the SFD. In another article, Smith (1996b) applied the Schur complement introduced by Haynsworth (1968) to divide the computational domain into some smaller subdomains.

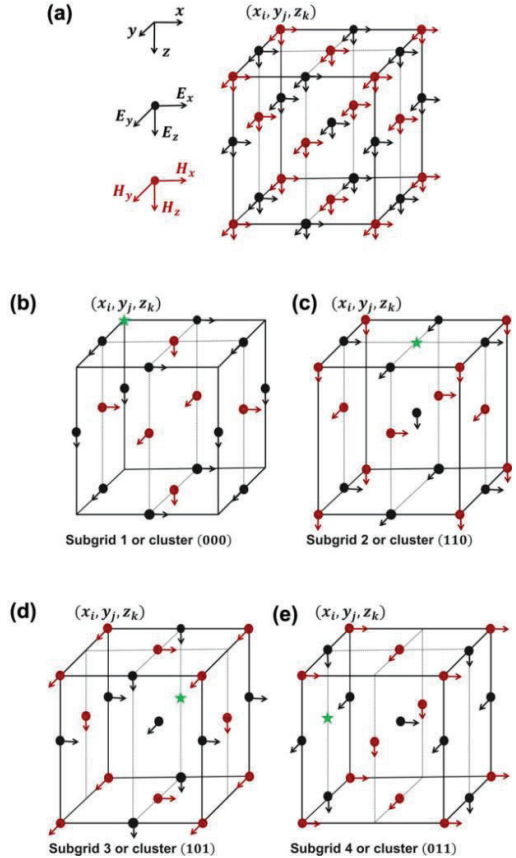
In the 1990s, the use of FD for EM researches on anisotropy of EM field still stayed in 2D. Pek and Verner (1997) proposed a FD algorithm of MT fields in 2D generally anisotropic block structures. At that time, the solution to the 2D anisotropy problem was still limited by computer performance. At the beginning of the 21st century, the study of the anisotropy problem of FD began to consider 3D models. Wang and Fang (2001) developed the SFD to simulate the multicomponent EM response in 3D inhomogeneous medium with arbitrary anisotropy. By using the coupled Maxwell's equation, the computation time of anisotropy was approximately equal to the isotropic calculation time. From another perspective, for simulation of EM induction in 3D anisotropic medium, Weiss and Newman (2002) proposed a new SFD algorithm which accurately simulated the effect of the geological structures on induction tool response. The new work extended the previous isotropic work by Newman and Alumbaugh (1995) to anisotropy and also effectively controlled the calculation cost of anisotropy to be similar to that of isotropy.

169 Gradually, the SFD has been widely applied in induction logging, borehole,
170 airborne and marine modeling. Followed the work by [Newman and Alumbaugh \(1995\)](#)
171 [and Alumbaugh et al. \(1996\)](#), [Newman and Alumbaugh \(2002\)](#) developed the SFD
172 approach for simulating the 3D induction logging response with quasi-static limit and
173 transverse anisotropy. The approach used the decoupled vector potential and dc scalar
174 potential functions. The new developed preconditioner significantly sped up the
175 solution of low induction numbers (LINs) and low frequency. Differently from
176 [Newman and Alumbaugh \(2002\)](#), [Hou et al. \(2006\)](#) proposed a new SFD algorithm
177 using coupled scalar-vector potential formulas. Averaged conductivities and potential
178 components not defined on the same points were calculated by the similar methods
179 used by [Wang and Fang \(2001\)](#) and [Weiss and Newman \(2002\)](#). The proposed
180 algorithm could efficiently and accurately simulate various types of the frequency and
181 arbitrary electrical anisotropy in the complex 3D borehole EM modeling. Applying
182 the SFD algorithm to the AEM system, [Liu and Yin \(2014\)](#) obtained the solution of
183 the coupled the partial differential equations (PDEs) for the scattered electrical fields.
184 They adopted the specifically designed divergence correction technique for the 3D
185 anisotropic model to accelerate the process of the simulation. The technique greatly
186 improved the calculation efficiency and the convergence speed of the solution. By
187 using the SFD method, [Li et al. \(2018\)](#) applied the complex frequency-shifted
188 perfectly matched layer (CFS-PML) boundary ([Kuzuoglu & Mittra, 1996](#)) to 3D
189 marine CSEM modeling. Compared to using the Dirichlet boundary condition, the
190 algorithm using the CFS-PML saved more computing time and memory and could be
191 more efficient.

192 *Lebedev grids*

193 The above mentioned SFDs are mostly based on Yee's SFD variants. Actually
194 before [Yee \(1966\)](#), [Lebedev \(1964\)](#) presented a different SG scheme. [Davydycheva](#)
195 [and Druskin \(1999\)](#) introduced Lebedev grids to solve the Maxwell's equation.
196 Differently from Yee grids, Lebedev grids places all components of the electric fields
197 at one set of nodes, and all components of the magnetic fields at another set of nodes.
198 This maintains the current conservation property in the grid cells and addressed the
199 modeling with anisotropy in the physical properties. Figure 3 shows the difference
200 between Lebedev grids and Yee grids. Lebedev grids can be split in four uncoupled
201 standard Yee grids but four times the computational cost is needed compared to the
202 similar isotropic problem in the standard Yee grids ([Wang and Fang, 2001](#); [Weiss and](#)
203 [Newman, 2002](#)). In order to reduce the cost of computation in the Lebedev grids,
204 [Davydycheva et al. \(2003\)](#) employed a proper averaging of the sources, solutions, and
205 error elimination and a spectrally optimal grid refinement scheme to calculate the
206 electromagnetic field of the 3D anisotropic inhomogeneous media in the EM
207 induction logging. The grid size was significantly reduced and the 3D calculation was
208 greatly accelerated without sacrificing accuracy. [Jaysaval et al. \(2016\)](#) also presented
209 an algorithm based on the Lebedev grid with a multigrid preconditioner for the
210 numerical simulation of 3D CSEM general electrical anisotropic conductive medium.
211 They accurately simulated layered and 3D tilted transverse isotropic (TTI) typical

212 marine CSEM model and proved the importance of considering the fully anisotropy of
 213 the conductivity tensor for the inversion. And a rule was observed that the solution
 214 time of a linear system increases linearly with the increase of unknowns.



215
 216 Figure 3. (a) Lebedev grid cell used to define the collocated electric and
 217 magnetic field components. (b) Standard Yee grid, and the complementary
 218 Yee grids constructed by shifting the components of E and H by half a cell in the (c)
 219 x-, (d) y- and (e) z-directions. (Jaysaval et al., 2016)
 220

221 2.1.2 FDTD

222 Finite-difference time-domain method (FDTD) has been widely applied into the
 223 simulation of the time-domain EM fields. It directly solves the Maxwell's equation in
 224 the time domain without requiring any form of derived equation. The prominent
 225 advantage of FDTD is that it can simulate various complex structures only by
 226 assigning the components of the EM fields contained by the difference format to each
 227 grid. Due to adopting the stepping method for calculation, FDTD can easily realize
 228 the simulation of various complex time-domain wideband signals, and it is very
 229 convenient to obtain the time-domain signal waveform at a certain point in space.

230 Goldman and Stoyer (1983) used the FDTD of a coaxial loop or wire loop
 231 transient electromagnetic (TEM) detection system to simulate the EM fields generated
 232 by a 2D buried cylindrical conductor. Based on the Du Fort-Frankel FD scheme (Du
 233 Fort and Frankel, 1953), Oristaglio and Hohmann (1984) applied FDTD to solve the

1
2
3
4
5
6
7
8
9
10
11
12
13
14
15
16
17
18
19
20
21
22
23
24
25
26
27
28
29
30
31
32
33
234 time-stepping Maxwell's equations in a 2D conductive earth. Wang and Hohmann
235 (1993) applied this method to the 3D TEM model. And in order to solve the boundary
236 conditions, Berenger (1994) first proposed the concept of FDTD perfectly matched
237 layer (PML) absorbing boundary conditions to calculate the boundary condition
238 problems in 2D time domain. Subsequently Katz et al. (1994) and Chew and Weedon
239 (1994) extended the FDTD PML to 3D time-domain calculations, and Debroux (1996)
240 applied the FDTD code to the 3D modeling of the EM response.

241 For reducing the computational time of 3D modeling, Commer and Newman
242 (2004) presented a parallel FDTD approach for 3D TEM modeling. By combining a
243 modified Du Fort-Frankel method with the FD scheme presented by Wang and
244 Hohmann (1993), Maxwell's equations were stepped in time. For simulating a real
245 large-scale earth model economically, the approach was parallelized to save the large
246 consumption of computational time. Maaø (2007) improved the FDTD based on
247 mathematical transformation rather than physical approximation (Oristaglio and
248 Hohmann, 1984) for marine-subsurface EM problem. The improvement significantly
249 reduced the frequency dependence of the propagation velocities and cut down the
250 computational time. Continuation of this mathematical transformation improvement,
251 Mittet (2010) presented a numerically cost-efficient high-order FDTD scheme, which
252 used a correspondence principle of wave and diffusion fields, for efficiently
253 simulating marine CSEM data. And de la Kethulle de Ryhove and Mittet (2014)
254 developed it to solve Maxwell's equations for marine MT 3D modeling. They pointed
255 out that the FDTD method completely avoided solving the linear system of equations.
256 It allowed the calculation of the unknowns of EM fields at all frequencies in only one
257 simulation, with very low computation complexity and low memory.

258 2.1.3 FDFD

34
35
36
37
38
39
40
41
42
43
44
45
46
47
259 Frequency-domain finite-difference method (FDFD) based on Maxwell's
260 equation is simple and intuitive in both principle and formulas, and can be used to
261 deal with various EM problems. However, the classic FDFD needs to discretize the
262 entire calculation area, and a difference equation must be established at each grid
263 node. In spite of the final matrix equation is sparse, the scale of the matrix will
264 increase rapidly as the computational domain increases, resulting in a huge burden of
265 calculation and storage. Therefore, FDFD is usually combined with some other
266 techniques to reduce the computational cost.

48
49
50
51
52
53
54
55
56
57
58
59
60
61
62
63
64
65
267 The most common combination of FDFD is the use of Yee grid to discretize the
268 EM fields. Mackie et al. (1994) combined the SFD algorithm with the minimum
269 residual relaxation method to calculate the MT response of general 3D models in the
270 frequency domain. Frequency-domain SFD has been used successfully to solve EM
271 fields in isotropic medium (Newman and Alumbaugh, 1995; Alumbaugh et al., 1996;
272 Smith, 1996a) and then has been developed into anisotropy (Wang and Fang, 2001;
273 Weiss and Newman, 2002; Hou et al., 2006). Even this method has been applied to
274 the forward modeling of the EM inversion problem (Egbert and Kelbert, 2012;
275 Grayver et al., 2013). It is worth noting that Egbert and Kelbert (2012) developed a
276 module system of computer codes, ModEM, for EM inversion. ModEM has already

277 been widely applied into 3D MT and CSEM problems (Kelbert et al., 2014).

278 FDFD is relatively simple and suitable for CSEM surveys which extracting only
279 a few discrete frequencies from data (Streich, 2009). Streich (2009) discussed the
280 iterative and direct solvers for solving the system of equations and used a massively
281 parallel sparse direct solver (MUMPS) (Amestoy et al., 2000) to solve the system of
282 equations from FDFD. The staggered scheme with electric-field components located
283 on the cell faces and the magnetic-field components on the edges was better for the
284 CSEM surveys than the more commonly used SG. Similarly, using the same scheme
285 described by Streich (2009), Grayver et al. (2013) applied FDFD and MUMPS in the
286 forward algorithm for 3D CSEM data inversion. Modern distributed-memory
287 platforms solved the high memory demand of the direct solver. In order to obtain a
288 stable system at low frequencies using a direct solver, a static divergence correction
289 (Smith, 1996b) was enforced for the static limit in the low-conductivity air layer.
290 However, it is not necessary for typical CSEM frequencies (~0.1-10Hz) (Streich,
291 2009; Jaysaval et al., 2014). And Jaysaval et al. (2014) applied a Schur complement
292 scheme (Haynsworth, 1968; Smith, 1996b) to FDFD with the commonly used
293 staggered scheme for fast multi-model 3D CSEM modeling. The Schur complement
294 system was solved by using MUMPS and the scheme overcame the shortcoming of
295 standard FDFD method, which required repeated forward modeling of the whole earth
296 model at each iteration, so that reducing the computation complexity greatly. The
297 efficiency of the FDFD code was validated against the FDTD code developed by
298 Maaø (2007) and Mittet (2010).

299 In addition, there are some other optimization schemes. Yavich and Zhdanov
300 (2016) developed a new efficient frequency-domain SFD method for calculating
301 discrete 1D layered background conductivity, based on introducing a contraction
302 operator (CO) to construct an effective FD EM-modeling preconditioner. The
303 contraction preconditioner can significantly accelerate the convergence of the FD
304 iterative solver and save the memory storage of the computation. Considering that
305 there is no need for fine grids in deep underground, Cherevatova et al. (2018)
306 presented a multi-resolution (MR) FD approach for frequency-domain 3D MT
307 forward modeling. The MR staggered-grid (SG) scheme was implemented to decrease
308 the horizontal resolution with depth. Three ways of handling the interface layers were
309 considered and the best one retained the symmetry of the coefficient matrix with a
310 similar accuracy result as the SG solution. Compared with the basic SG, MR scheme
311 improved the computation efficiency without the loss of the solution accuracy.
312 Varilsuha and Candansayar (2018) studied different EM formulation approaches,
313 including direct EM formulation, ungauged and gauged (Lorenz, Coulomb, and axial)
314 vector and scalar potential formulations, to solve the problems of 3D MT modeling.
315 Comparing the accuracy and the speed of the FD solution for each method, the
316 ungauged method provided faster simulation with the same precision. Furthermore,
317 the axial specification system forward modeling also had a faster speed of CSEM
318 field simulation than other methods.

319 2.1.4 2.5D problem

1
2
3
4
5
6
7
8
9
10
11
12
13
14
15
16
17
18
19
20
21
22
23
24
25
26
27
28
29
30
31
32
33
34
35
36
37
38
39
40
41
42
43
44
45
46
47
48
49
50
51
52
53
54
55
56
57
58
59
60
61
62
63
64
65

320 Although the use of high-performance computing can achieve 3D forward
321 modeling, the cost of discretizing the computation domain of fully 3D models is
322 extremely expensive. To avoid direct 3D solution, there is a reasonable assumption
323 that the geological structure with topography within a certain range is a 2D model
324 with uniform electromagnetic characteristics in the strike direction. It should be noted
325 that such an assumption is not suitable for discussing fully anisotropy. The coordinate
326 in the strike axis is transformed into the wavenumbers by Fourier transforms. For each
327 of a number of wavenumbers, only a 2D problem need to be solved (Stoyer and
328 Greenfield, 1976) and the response is still that of a 3D model with the properties
329 invariant along one of the axes. Such 2D problem is described as 2.5D problem and it
330 simplifies the 3D solution and significantly reduces the number of unknowns and
331 computational cost. The 2.5D problem also applies to FEM and IE that will be
332 reviewed in the corresponding section later.

333 The 2.5D FD method was first proposed by Stoyer and Greenfield (1976).
334 Abubakar et al. (2006a) put forward a 2.5D SFD forward algorithm for marine CSEM.
335 The algorithm solved all source-receiver configurations simultaneously, which greatly
336 improved the calculation efficiency and helped the realization of fast inversion
337 algorithms. Based on Abubakar et al. (2006a), Abubakar et al. (2008) presented
338 efficient 2.5D forward and inversion algorithms for the interpretation of
339 low-frequency EM measurement. And the forward algorithm used a multifrontal LU
340 decomposition (Davis and Duff, 1997) to invert the stiffness matrix. Chen et al. (2011)
341 developed a 2.5D SFD code for simulating the responses of logging-while-drilling
342 (LWD) deep directional EM tools and wireline tensor induction tools in high angle
343 and horizontal (HA/HZ) wells. The code was applied for 2D formation conductivity
344 distributions and 3D well trajectories. Zeng et al. (2018) proposed a 2.5D FD method
345 based on Yee's grid using the weighted average method (Weiss and Newman, 2002)
346 to simulate the anisotropy of 2D resistivity logging. The Fourier transform was
347 performed by adopting the Gauss-Legendre quadrature rule and the inverse Fourier
348 transform was accelerated by employing the Gaussian quadrature method (Quarteroni
349 et al., 2010), which greatly reduced the calculation time and improved the
350 computation efficiency. This made the 2.5D FD has a better applicability than 3D
351 scheme.

352 Above all, FD is a simple and practical numerical simulation method for solving
353 PDEs by approximating the derivative with a difference. Because of the approximate
354 solution obtained by differential approximation and interpolation, FD has the
355 advantage for the general model. Due to the own characteristics of the SG, the SFD
356 method can largely solve the problems of EM fields discontinuity caused by the
357 difference in electromagnetic properties of the medium. FDTD and FDFD have
358 different applicability and whether in the time or frequency domain, the whole
359 domain needs to be discretized so that FD is not suitable for solving more complex
360 domains. In addition, since the interpolation calculation is in the whole domain,
361 different discretized grid sizes will get different solution results.

1
2
3
4
5
6
7
8
9
10
11
12
13
14
15
16
17
18
19
20
21
22
23
24
25
26
27
28
29
30
31
32
33
34
35
36
37
38
39
40
41
42
43
44
45
46
47
48
49
50
51
52
53
54
55
56
57
58
59
60
61
62
63
64
65

362 **2.2 Finite element method**

363 Finite element method (FEM) is based on the variational method and the
364 weighted equivalent integral method. According to the principle of variation or the
365 principle of orthogonalization between the remainder of the equation and the weight
366 function, an integral expression equivalent to the initial boundary value problem of
367 the differential equation is established. Although both belong to the DE method, FEM
368 is very different from FD. In the process of solving, an interpolation function is used
369 to connect all the discrete units, and the PDEs group becomes a total stiffness matrix
370 to be solved. No matter how complicated the calculation domain is, it can be
371 discretized into finite elements and these elements are connected through interpolation
372 functions to realize the solution of the complex domain.

373 Originally FEM was applied to solve the elastic and structural analysis problems
374 (Hrennikoff, 1941; Courant and Robbins, 1942). Until the 1970s, Coggon (1971)
375 firstly employed it to calculate EM fields. Rodi (1976) proposed the FEM for a
376 numerical simulation of MT data on 2D conductivity model with a new rectangular
377 grid. Rijo (1977) put forward a single-module FEM algorithm which can deal with 2D
378 symmetry problems in electromagnetic methods. This algorithm greatly improved the
379 accuracy and the speed of 2D EM simulation. Wannamaker et al. (1986) employed
380 this method to simulate the 2D MT response with terrain. These methods can be used
381 to simulate both the MT and the CSEM data. In 3D space, the computational cost of
382 FEM for simulating 3D EM response increased dramatically. The limitation of
383 computer operation speed and physical memories hindered the usage of FEM. Since
384 1980s, 3D EM modeling methods have been gradually proposed with the
385 development of computational resources (Pridmore et al., 1981; Mur, 1991).
386 Considering the huge computational burden of 3D EM modeling, Zyserman and
387 Santos et al. (2000) applied parallel FEM 3D EM modeling.

388 **2.2.1 Mesh generation technology**

389 Since mesh generation is a very important step in FEM numerical analysis, and it
390 directly affects the accuracy of the subsequent numerical calculation and analysis
391 results, the predecessors have fully studied this technology.

392 The structure mesh is generated fast with high quality and it can be easily applied
393 to simulate curves or surfaces only by parameterized methods or interpolation
394 (Wannamaker et al., 1987). However, this also limits its scope of application, making
395 it inadequate for calculations in complex domains. In order to overcome limitations of
396 computational complexity and the inherent constraints of EM fields, structured-grid
397 FEM were proposed in some reviews (Sugeng, 1998; Yoshimura and Oshiman, 2002).

398 Compared to structured grid, unstructured grid can accurately segment curved
399 boundaries of complex geological structures such as terrain or seafloor topography
400 because of the flexibility of meshing and reduce the size of the system of linear
401 equations arising from the forward problem (Börner et al., 2008; Schwarzbach and
402 Haber, 2013).

1
2
3
4
5
6
7
8
9
10
11
12
13
14
15
16
17
18
19
20
21
22
23
24
25
26
27
28
29
30
31
32
33
34
35
36
37
38
39
40
41
42
43
44
45
46
47
48
49
50
51
52
53
54
55
56
57
58
59
60
61
62
63
64
65

403 Unstructured grid generation technology solves the discretization of complex
404 calculation domains while the speed and quality of mesh generation will decrease and
405 the difficulties in boundary recovery will also be introduced. In order to prevent
406 excessive meshing and find the optimal meshes, adaptive mesh refinement technology
407 is an effective method to solve this problem.

408 **2.2.2 Adaptive FEM.**

409 The adaptive FEM is a numerical method that can automatically adjust the
410 algorithm through adaptive analysis to improve the solution process. It is based on the
411 conventional FEM, with a posteriori error estimation and adaptive mesh improvement
412 technology. The method can successfully save physical memories and significantly
413 improve the computational efficiency and accuracy.

414 [Key and Weiss \(2006\)](#) applied the adaptive FEM for 2D MT modeling. They
415 replaced the rectangular grids with irregular triangular grids since it was easier to
416 simulate complex structural boundaries. The adaptive refinement method based on the
417 dual-error weighting approach (DEW) ([Ovall 2006](#)) refined the mesh with insufficient
418 precision through iteration in order to ensure the accuracy. [Li and Key \(2007\)](#) applied
419 the DEW approach into 2.5D marine CSEM, enabling the unstructured grids to adjust
420 themselves automatically to calculate EM fields effectively. Since the analytical solution
421 is used to calculate the primary field, it was the most accurate solution during that
422 time. [Li and Pek \(2008\)](#) presented a similar goal-oriented self-adaptive FEM with
423 DEW as a guide. The algorithm improved the quality of numerical solutions in a
424 general 2D MT anisotropic conductivity media. For 3D case, [Ren and Tang \(2010\)](#)
425 presented an adaptive FEM for direct current (DC) resistivity modeling. It started with
426 the initial coarse mesh and then based on a gradient recovery scheme. The mesh
427 refined adaptively according to the indication of a recursive error estimator. The
428 whole process of adaptation is shown in Figure 4. Where CFEM is the abbreviation of
429 conventional finite element method, $\overline{\eta_e}$ is the average element error percentage, and
430 η^* is the given error criterion. [Schwarzbach et al. \(2011\)](#) proposed a 3D adaptive
431 higher order FEM for modeling a realistic marine CSEM scenario. The adaptive mesh
432 refinement strategy and the higher-order polynomial (HOP) FEM improved the
433 accuracy of the solution.

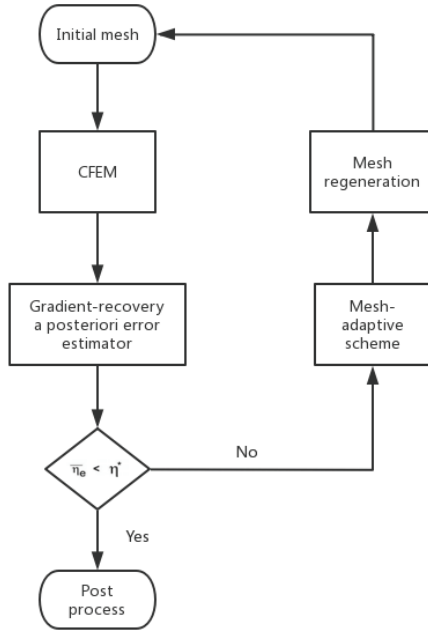
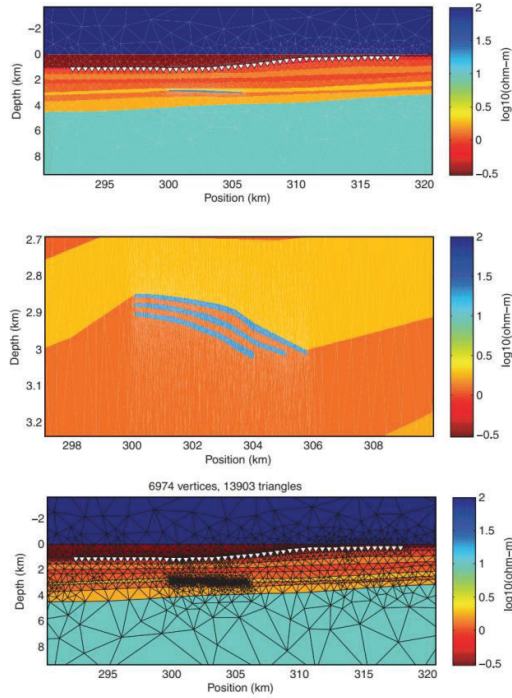


Figure 4. The whole process of the adaptive FEM scheme. (Modified from Ren and Tang, 2010)

Actually, according to the posterior error estimation method, the adaptive mesh refinement technology can be divided into two types. One is based on the super-convergence characteristic of the variant of the EM field (Key and Weiss, 2006; Ren and Tang, 2010; Schwarzbach et al., 2011). The other is based on the continuity of the EM field or the current density (Yin et al., 2016). Ren et al. (2013) applied the continuity-condition-based adaptive FEM for plane wave 3D EM modeling based on electric field differential equations. And then, Yin et al. (2016) presented a goal-oriented, continuity-condition-based adaptive FEM for 3D scattered AEM modeling in the frequency domain. In addition, Zhang et al. (2018) employed the method with the backward Euler scheme to perform time-domain 3D airborne full-wave EM field simulation. The random grid-selection technique improved the stability of the forward modeling and controlled the number of meshes in the adaptive process, thereby the efficiency of EM simulation was improved.

In fact, Ovall (2006) also proposed another called the dual weight residual (DWR) method. Compared to the DEW method, the DWR method calculated the weight of residual instead of the gradient recovery. In other words, DWR replaced the absolute error of DEW with the relative error. Such a goal-oriented refinement strategy could dramatically reduce the density of adaptive refinement grids to a greater extent and save more a large number of computational resources while keep high numerical accuracy. Therefore, Key and Ovall (2011) developed a parallel goal-oriented adaptive meshing technique based on the DWR method and implemented this technique into a parallel Fortran code named Modeling with Adaptively Refined Elements for 2D EM (MARE2DEM). Figure 5 shows a typical synthetic marine CSEM model for hydrocarbon exploration on the continental shelves. The technique was tested and proved on this model. The optimal distribution of mesh

462 density was discovered and the accuracy of 2.5D EM numerical simulation was
 463 improved. The MARE2DEM software, Key (2016) published, also applied the
 464 method to automatically generate and refine an unstructured triangular element mesh
 465 for forward modeling and inversion. It ensured the accurate model response with
 466 various conductivity parameters. Liu et al. (2018b) put forward a goal-oriented
 467 adaptive FEM algorithm for 3D MT modeling in generally anisotropic conductivity
 468 media. A global residual based posterior error estimator was employed to guide the
 469 refinement of unstructured tetrahedral meshes. The algorithm realized the modeling of
 470 arbitrary bathymetries and structural boundaries.



471
 472 Figure 5. Complex marine conductivity model including typical features that are
 473 difficult to discretize on a rectangular grid: a large bathymetric slope, tilted regional
 474 strata and closely spaced thin and dipping reservoir intervals. The three panels show
 475 the model (top panel), a close-up of the stacked reservoir layers (middle panel, note
 476 the vertical exaggeration) and the unstructured grid used as the starting mesh (bottom
 477 panel). Inverted white triangles show the location of the seafloor EM receivers. Only
 478 the central portion of the model is shown (Key and Oval, 2011).

479 The unstructured grid solves the complexity of the solution area, and the
 480 adaptive scheme solves the problem of grid division, so that they have improved the
 481 calculation accuracy and calculation efficiency of the finite element solution process
 482 to a certain extent. However, due to the diffusion of the EM field itself, the
 483 convergence rate of the solution has not been resolved.

484 2.2.3 More optimization solutions

485 *Divergence correction*

1
2
3
4
5
6
7
8
9
10
11
12
13
14
15
16
17
18
19
20
21
22
23
24
25
26
27
28
29
30
31
32
33
34
35
36
37
38
39
40
41
42
43
44
45
46
47
48
49
50
51
52
53
54
55
56
57
58
59
60
61
62
63
64
65

486 Due to the characteristics of electric field diffusion, the speed of convergence,
487 especially at low frequencies, was very slow with the low convergence rate.
488 Farquharson et al. (2011) proposed a divergence correction method applied in the
489 FEM based on Smith (1996b) on divergence correction. This correction method
490 promoted the process that the discontinuous conductivity in the approximate electric
491 field generated the discontinuous normal component. The convergence speed of the
492 equations was accelerated and the computation efficiency was improved. Kordy et al.
493 (2016) described the divergence correction as the typical procedure for removing
494 spurious curl-free fields caused by current divergences over the discretized model
495 domain during the iterative solution process.

496 *Edge-based or Vector FEM*

497 The conventional FEM has an obstacle that the node-based FEM cannot handle
498 the discontinuity of the normal electric field component. One solution is to use the
499 electromagnetic potential formulation (Badea et al., 2001). Because the electric field
500 can be decomposed into vector and scalar potential in Helmholtz equation and the
501 charge conservation equation, Mitsuhashi and Uchida (2004) proposed a FEM method
502 for 3D MT conductivity response based on the T- Ω Helmholtz decomposition. In
503 particular, the vector field T is approximated by the twelve components assigned at
504 the centers of edges of each element and the scalar field Ω is approximated by the
505 eight components at the vertices of each element. Mukherjee and Everett (2011) put
506 forward an edge-based tetrahedral mesh FEM algorithm based on an ungauged
507 potential formulation to simulate near-surface 3D CSEM induction response, which
508 addressed local inhomogeneities in the electrical conductivity and magnetic
509 permeability distribution near the surface.

510 However, potential formulation may introduce more numerical instability
511 (Puzyrev et al., 2013). Ansari and Farquharson (2014) proposed an unstructured
512 tetrahedral mesh vector FEM solution for frequency domain 3D EM modeling. The
513 discretization of the edge element and node element were used to approximate the
514 vector potential and the scalar potential, respectively. The scheme adopted the
515 Galerkin method (Jin, 2002) variant of the weighted residual method to discretize the
516 equations of the sparse linear system, and applied the generalized minimum residual
517 solver with incomplete LU preprocessor (Saad, 2003) to solve the system iteratively.
518 Based on this scheme, Ansari et al. (2017) proposed a new gauged finite-element
519 potential formulation for 3D EM modeling. The block diagonal preprocessing scheme
520 based on the Schur complement of the potential system stabilized the iterative
521 solution of the estimation system. Both the iterative solution and the direct solver had
522 the same response to the potential, which proved the uniqueness of the potential
523 solution. And then Dunham et al. (2018) employed the 3D finite element code
524 provided by Ansari and Farquharson (2014) to the real exploration prospects of the
525 Flemish Pass basin offshore Newfoundland, Canada, and extended the application of
526 FEM for the 3D marine CSEM. Models were discretized with unstructured tetrahedral
527 meshes. The edge length constraints as an optimization reduced the total number of
528 tetrahedral elements and refined specific areas of the mesh. It accurately simulated the

529 complex structures in the model, simultaneously minimizing the numbers of model
530 unknowns.

531 Another solution is using edge-based FEM (Nédélec, 1980; Jin, 2002). The use
532 of edge elements can ensure the continuity across different medium of the vector basis
533 function, while ensuring zero curl and non-zero divergence, and can ideally express
534 electromagnetic physical characteristics such as current density. Edge-based FEM is
535 also known as vector FEM. Since the vector FEM could satisfy the discontinuity of
536 the normal component of the electric field, the advantage of retaining the calculation
537 accuracy and high computation efficiency is to avoid the divergence correction. Nam
538 et al. (2007) used vector FEM to realize 3D MT forward modeling. Liu et al. (2008)
539 applied the unstructured grid to improve the method which used the vector FEM to
540 efficiently simulate the 3D MT response and it further improved the forward
541 modeling accuracy.

542 In order to increase modeling efficiency while ensuring accuracy of 3D CSEM
543 modeling, da Silva et al. (2012) introduced MUMPS into the edge-based FEM for
544 solving the linear system of equations. The scheme of non-uniform Cartesian
545 conforming hexahedra made the grid generation more convenient. And it was
546 demonstrated that the presented approach was robust for indefinite and ill-conditioned
547 linear systems. Chung et al. (2014) used edge-based FEM based on a hexahedral mesh
548 with a direct solver PARDISO (Schenk and Gärtner, 2004) for 3D CSEM modeling.
549 The results of a series of comparative experiments verified the effectiveness of the
550 edge-based FEM and the advantages of the direct over iterative solver. However, both
551 da Silva et al. (2012) and Chung et al. (2014) indicated that there was a limitation in
552 the hexahedral mesh when the model complexity increased and maybe a tetrahedral
553 mesh could be adopted. Li et al. (2016) combined the total-field algorithm, local
554 refinement of unstructured tetrahedral mesh and vector FEM for EM modeling. The
555 MUMPS was used to solve the linear equations. And differently from the unnecessary
556 large distances to the truncation boundaries as Chung et al. (2014) set, appropriate
557 truncation boundaries for the computational domain was determined by numerical
558 experiments which reduced the waste of calculations to a certain extent.

559 Utilizing the computation power of modern distributed-memory platforms, Ren
560 et al. (2014a) developed a new parallel vector FEM code combined with unstructured
561 meshes for plane wave 3D EM modeling. Based on a domain-decomposition
562 approach, the code recombined the unknowns. Parallel implementation used the
563 robust direct solver PARDISO. Compared with the traditional FEM, the code could
564 solve more complicated large-scale models. Grayver and Bürg (2014) also studied a
565 robust and scalable approach for large-scale 3D EM modeling in the frequency
566 domain. They applied the flexible generalized minimal residual (FGMRES) iterative
567 Krylov subspace method (Saad, 2003), which significantly reduced the computational
568 time and memory. However, both Ren et al. (2014a) and Grayver and Bürg (2014)
569 only employed the lowest order Nédélec elements (Nédélec, 1980). Grayver and
570 Kolev (2015) extended the Grayver and Bürg (2014) approach to the arbitrary order.
571 Combining the high-order FEM with the relationship of target local mesh, the
572 computation time was saved and at the same time, the multi-degree of freedom

1 573 calculation was also reduced. Based on these works, [Grayver \(2015\)](#) employed
2 574 adaptive FEM on parallel 3D MT modelling and inversion. The adaptive mesh
3 575 refinement technology avoided over-parameterization and accurately calculated the
4 576 EM response based on goal-oriented error estimator. The computation effort was
5 577 significantly saved by a locally refined decoupling grid and the calculation of the
6 578 electromagnetic field at each frequency using an independent grid further improved
7 579 the computation efficiency. Then, [Grayver et al. \(2019\)](#) applied it combined with
8 580 high-order meshes to calculate the high-resolution solution of 3D MT modelling in
9 581 spherical earth.

12 582 The above papers are all discussions on isotropic media. Some differently, [Cai et](#)
13 583 [al. \(2014\)](#) presented a linear edge-based FEM for the numerical simulation of the 3D
14 584 CSEM data in anisotropic conductive medium. The scheme used a non-uniform
15 585 rectangular mesh to capture the rapid changes of the diffused electromagnetic field in
16 586 the abnormal conductivity region and around the source, which also can be
17 587 transformed to hexahedral mesh to simulate the effect of sounding. Later, based on the
18 588 previous work, [Cai et al. \(2017a\)](#) employed total field formulation and unstructured
19 589 tetrahedral mesh. A new hybrid boundary condition was used to reduce the
20 590 computation domain while improve the accuracy of forward modeling. The MUMPS
21 591 was used to speed up the solution of the system of equations.

26 592 [Castillo et al. \(2016\)](#) developed an edge-based FEM parallel code for the
27 593 isotropy of 3D marine CSEM forward modeling. The scalability testing and the
28 594 evaluation of the error norm of the different size meshes verified that the method still
29 595 maintained high accuracy with good parallel efficiency. And then, [Castillo et al. \(2018\)](#)
30 596 developed a Parallel Edge-based Tool for Geophysical Electromagnetic modeling
31 597 (PETGEM), which is the first open-source modeling toolbox for 3D marine CSEM
32 598 problems, to study the 3D CSEM problem of an infinitesimal dipole arbitrary
33 599 isotropic medium with low frequency approximation. They provided an adaptive
34 600 scheme for frequency and specific source locations, and developed a scalable study of
35 601 HPC architecture based on basic metrics. However, PETGEM only support first-order
36 602 polynomials, isotropy and cannot process the multiple horizontal electric dipoles
37 603 without surface topography. Therefore, [Rochlitz et al. \(2018\)](#) developed an
38 604 open-source toolbox custEM (customizable electromagnetic modeling) for complex
39 605 3D CSEM modeling. The custEM is similar to the PETGEM but support HOP,
40 606 anisotropy and multiprocessing.

47 607 *Time-domain finite-element method*

50 608 For simulating transient EM fields in 3D diffusive earth media, [Um et al. \(2010,](#)
51 609 [2012\)](#) put forward a time-domain finite-element method (FETD). An unstructured
52 610 grid and adaptive time-stepping doubling (ATSD) scheme was used to simulate the
53 611 diffusion of 3D electromagnetic waves. Compared with the analytical method and the
54 612 3D FDTD, the algorithm was demonstrated. Although the FETD with unstructured
55 613 grid and ATSD have a potential to reduce the number of unknowns and time steps, the
56 614 FETD method was often difficult to extend with available parallel computing
57 615 resources, due to each step required solving a large-scale unstructured sparse matrix.

616 Fu et al. (2015) designed a parallel FETD method for improving modelling speed.
617 Multi-threading sped up the key steps of solving large sparse matrices and the
618 convergence, and greatly reduced computation time while ensuring accuracy. Cai et al.
619 (2017b) implemented FETD with a hybrid boundary condition to simulate CSEM data.
620 They employed the unstructured tetrahedral mesh to discretize the model domain and
621 adopted the ATSD to keep the same step size. Then, the semi-adaptive method was
622 also adopted to discrete the model domain. The new hybrid boundary condition used
623 the primary field corresponding to the layered background model to approximate the
624 total field on the boundary. Additionally, based on the unstructured tetrahedral mesh
625 and the ATSD scheme, Cai et al. (2017c) also developed an adaptive Padé series
626 method (Baker and Graves-Morris, 1996) to approximate the Cole-Cole model. The
627 method improved the accuracy of the Padé approximation over a wide time range to
628 enhance the simulation accuracy. Applying the edge-based FEM for the spatial
629 discretization and the second-order of backward Euler scheme for the time
630 discretization (Um et al., 2010), Liu et al. (2019) adopted the direct solver MUMPS to
631 factorize the large sparse matrices obtained by FEM and utilized the iteration scheme
632 from an initial field for all time channels to solve the TEM forward modeling with
633 topography using unstructured tetrahedral grids efficiently.

634 2.2.4 2.5D problem

635 As early as 1985, Lee and Morrison (1985) have already used 2.5D FEM for the
636 electromagnetic scattering by a 2D inhomogeneity. Everett and Edwards (1992),
637 Unsworth et al. (1993), and Mitsuata (2000) applied 2.5D FEM to obtain the EM
638 induction over a 2D earth. The previously mentioned papers, such as Li and Key
639 (2007), Key and Owall (2011) and Key (2016) applied the 2.5D FEM into the
640 simulation of the marine EM. Kong et al. (2008) also presented a 2.5D FEM
641 difference method for marine CSEM in stratified anisotropic media. Kang et al. (2012)
642 used a 2.5D FEM to calculate the secondary field caused by a subsurface anomalous
643 for marine CSEM response.

644 In general, FEM is an effective forward modeling method with high precision of
645 simulation. More degrees of freedom for meshing enables FEM to solve the problem
646 that the FD method cannot cope with complex solution domains. However, the
647 property of the mesh will sacrifice some simulation speed to some extent. With the
648 development of unstructured grids, adaptive schemes and parallel computing, the
649 simulation speed of FEM has been solved partially, which makes the precision
650 advantage of FEM more obvious than other forward methods. This is why researchers
651 are gradually interested in the study of FEM after 2000, what we have mentioned in
652 Section 1. At present, geophysicists have tried to combine the FEM with other
653 methods for more efficient forward modeling with high precision and high speed.

654 2.3 Integral equation method

655 Integral equation method (IE) is a method for solving the unknowns of the model

656 using integral equations. Usually, the Maxwell's equations in the form of differential
657 equations are converted into integral equations, and then applied the Green's function
658 (Wait, 1962) to obtained the scattering equations (SE). The linear system is generated
659 by the discretization of the SE and the solution to the forward modelling is the
660 solution to the linear system. However, differently from the discretizations of the DE
661 method (FD and FEM), IE only meshes the scattering area, that is the anomalous
662 bodies, instead of the whole computational domain. The efficiency advantage of IE is
663 critical to save the computation time of EM modeling, especially for simple 3D
664 models.

665 Integral equation method (IE) was first proposed by Hohmann (1971) for solving
666 2D inhomogenous EM response. And then, Hohmann (1975) developed a volume
667 integral equation method (VIE) based on a hexahedral mesh in order to calculate the
668 3D induced polarization and EM responses.

669 2.3.1 VIE

670 Volume integral equations method (VIE) is a very useful method for simulating
671 3D EM models. On the basis of the works done by Hohmann (1975), a series of
672 studies about the VIE had been conducted. Ting and Hohmann (1981) used a
673 structured grid to perform 3D MT forward modeling. And then, Hohmann (1983)
674 improved the general 3D IE solution by using the vector-scalar potential method and
675 introducing symmetry through a series of theories. Wannamaker et al. (1984) used IE
676 to simulate 3D EM response in a layered structure. SanFilipo and Hohmann (1985)
677 established a time-domain integral equation for TEM response in a restricted region of
678 half-space electrical conductors with anomalous conductivity.

679 Because of the limitation of the computation condition at that time, some
680 improved methods were developed. Wannamaker (1991) abandoned the original
681 charge estimation formula (Wannamaker et al., 1986) and utilized the real surface
682 charge with the potential difference. The improvement maintained the internal
683 consistency of the pulse basis function, meanwhile obtained a good approximation
684 result. So that the IE forward modeling of the 3D MT response could further deal with
685 the complex model structure. Differently from SanFilipo and Hohmann (1985),
686 Walker and West (1991) proposed an IE solution that could stably simulate the EM
687 scattering of thin plates. It was suitable for scattering models in fully resistive or
688 conductive medium. The uncertainty of the solution was eliminated by the robustness
689 of the IE solution, so this method had a strong applicability to simulate broadband EM
690 response.

691 In order to overcome the limitation of discretization cells number caused by the
692 restriction of the computer memory, Xiong (1992) developed a new IE for the
693 simulation of 3D earth conductivity structure. The scattering matrix was divided into
694 multiple sub-matrices, and the block iteration method was used to solve the whole
695 system, which greatly reduced the calculation time of solving matrix equations.
696 Because each sub-matrix was independent of each other, the method also had a
697 potential for parallelization. And then, continued the works of Xiong (1992), Xiong
698 and Tripp (1993) used the spatial homogeneity and the symmetry relationship of the

699 Green's tensor (Wannamaker et al., 1984) to greatly reduce the computing time.

700 Actually, due to computer memory level restrictions in the 1980s, Singer &
701 Fainberg (1985) have already proposed an iterative dissipative method (IDM) applied
702 into integral equation based on a contraction operator, which was introduced by
703 Fainberg & Zinger (1980). The IDM was mostly adopted at that time; however, the
704 convergence of the method was slow. Then, Singer (1995) improved it and put
705 forward a modified iterative dissipative method (MIDM). On this basis, Singer (2008)
706 developed a new complex 3D EM fields modeling code, and employed the iterative
707 perturbation approach to generate a series of convergence solutions. The solution
708 optimization in the Krylov subspace significantly reduced the number of iterations,
709 meanwhile weakened the dependence on the lateral contrast of the model, so that the
710 accuracy, robustness and efficiency of the code was ensured.

711 In addition, combining the MIDM proposed by Singer (1995) and the Krylov
712 subspace iterative solution scheme (Krylov, 1931), Avdeev et al. (1997, 1998, 2002)
713 applied a 3D frequency-domain solution based on the VIE to simulate the response of
714 MT, CSEM, AEM and induction logging. Following these works, Avdeev and
715 Knizhnik (2009) improved the solution for modeling 3D EM fields by using its
716 inherent 3×3 dyadic Green's tensor (Avdeev et al., 1997) separability. The linear
717 dependence on all three dimensions overcame the quadratic dependence of the
718 traditional IE on the size of the model, not requiring the calculation or storage of the
719 entire Green's matrix. Thereby, the improvement significantly reduced the
720 computation load and improved the computation efficiency.

721 From another perspective of improvement, Farquharson and Oldenburg (2002)
722 studied the application of edge element basis vectors in the IE solution of 3D
723 electromagnetic simulation, and realized the edge-element basis function in the
724 numerical solution of the electric field integral equation. The system of equations was
725 solved by using the Galerkin approach. Later, Farquharson et al. (2006) employed the
726 electric-field VIE to calculate the numerical results of EM response, and implemented
727 the agreement of the numerical modeling and physical scale modeling results.

728 2.3.2 IE based on a contraction operator

729 The contraction operator mentioned earlier is from Banach theorem. The theorem
730 allows bounded linear operators defined on a certain vector space to expand to the
731 entire space, and states that there are "sufficient" continuous linear functions. That
732 means if operator is a contraction operator, successive iterations converge. Therefore,
733 the contraction operator will accelerate the convergence of the solution of the integral
734 equation.

735 By using IE based on a contraction operator, Zhdanov and Fang (1996) presented
736 a new approach called quasi-linear (QL) approximation to solve the EM induction
737 problem. The QL approximation was able to accurately estimate the broadband EM
738 response and had the potential to be applied into the fast 3D EM inversion. Similarly,
739 Zhdanov et al. (2000) proposed a quasi-analytical (QA) approximation method for
740 electromagnetic forward modeling based on the IE of scattering current. The
741 approximate solution was proposed by constructing the quasi-analytical expressions

742 of the anomalous EM fields for 2D and 3D models. The new method adopted iterative
743 methods to extend the quasi-analytic method and developed the approximation into
744 high order, which improved the accuracy. As a result, quasi-analytic series were
745 obtained. The stability and efficiency of the method were guaranteed by the improved
746 accuracy of the simulation and the greatly accelerated convergence speed of the
747 calculation. [Hursan and Zhdanov \(2002\)](#) presented a contraction integral equation
748 (CIE) technique, which replaced the original IE with the modified Green's operator
749 equation. The CIE technique significantly improved the convergence of the iterative
750 method. Later, it was developed into parallel by [Čuma et al. \(2017\)](#), and the fast
751 forward modeling has been implemented to a large extent. In order to improve the
752 validity of IE method for complex model calculation, [Zhdanov et al. \(2006\)](#) developed
753 a new IE method for 3D EM modeling in the complex structures with inhomogeneous
754 background conductivity. The new method overcame the limitation of traditional IE
755 which only used to simulate horizontal layered backgrounds, and improved the
756 calculation accuracy by iterative methods.

757 **2.3.3 Effective 3D numerical solvers**

758 Three-dimensional interpretation of EM data from different sources and scales
759 was increasingly becoming the key to 3D EM data analysis. However, in terms of the
760 computation complexity, accuracy and actual level of spatial detail, 3D EM numerical
761 simulation still existed challenge.

762 In view of this, using an effective 3D numerical solver was a good solution. [Sun
763 and Kuvshinov \(2014\)](#) proposed a method of Green's function matrix compression
764 based on singular value decomposition (SVD), which was used to accelerate the
765 solution of global geomagnetic induction by the electromagnetic IE forward solver.
766 The method significantly reduced the memory usage and Central Processing Unit
767 (CPU) time of the Krylov subspace iterative solution scheme under the premise of
768 less precision sacrifice. Similarly, Kruglyakov had done some work committing to the
769 optimization of IE forward solver for 3D modeling. [Kruglyakov et al. \(2016\)](#)
770 developed a new open-source 3D MT forward solver based on the CIE method. The
771 solver could accurately calculate the Green's function ([Ting and Hohmann, 1981](#)) and
772 its integral, at the same time it could solve high-contrast complex models and support
773 massive parallelization. Furthermore, [Kruglyakov and Bloshanskaya \(2017\)](#)
774 developed a new parallel VIE solver. The Galerkin method was used to ensure the
775 convergence of numerical solutions with high precision, stability and high
776 parallelization. Memory usage was eight times lower than other VIE solvers ([Avdeev
777 et al., 1997; Hursan and Zhdanov, 2002](#)). The solver had no additional restrictions on
778 the background media, so that it could achieve non-uniform discretization in any
779 layered background and vertical direction. On this basis, [Kruglyakov and Kuvshinov
780 \(2018\)](#) cooperatively proposed a new 3D numerical solver, which used HOP to
781 improve computation efficiency and greatly reduced the number of unknowns under
782 the premise of ensuring accuracy. The solver sped up the calculation and saved the
783 computing memory significantly.

784 **2.3.4 2.5D problem**

785 Several 2.5D EM forward modeling studies have been mentioned (Li and Key,
786 2007; Key and Owall, 2011; Zeng et al., 2018). Something different for IE is that after
787 Fourier transformation in the invariant direction, for each Fourier parameter, the
788 problem is reduced to the problem of solving 2D integral equations (Abubakar et al.,
789 2006b).

790 Abubakar et al. (2006b) proposed an IE forward algorithm for the solution of
791 2.5D low-frequency electromagnetic response over the scattering domain. The
792 algorithm employed a standard conjugate gradient normal residual method (CGNR) to
793 solve the linear system of equations and simplified the 3D problem by Fourier
794 transform into solving multiple 2D integral equations, which greatly reduced the
795 computation complexity. Dyatlov et al. (2015) developed and successfully validated a
796 boundary integral equation algorithm based on the four tangential components of the
797 electric field and magnetic field for simulating the response of the LWD EM tool in
798 complex 2D and 3D structures. The Fourier transform simplified the high dimension
799 problems into a series of 1D frequency-independent integral equation, and
800 simultaneously calculated the whole set of measurement points with the same matrix,
801 which greatly shortened the calculation time. The boundary integral equation method
802 avoided the so-called near-offset problem of 2.5D FD simulation with singular
803 sources and had a potential for parallelization. Then, Dyatlov et al. (2017) improved
804 this method in a 2D model with plane boundaries, and calculated the solution of the
805 two-layer model (TLM) corresponding to the nearest boundary by explicit formula.
806 The solutions of the TLM improved the computation accuracy while maintaining the
807 original computation efficiency when the transmitter and the boundary were close.
808 However, when the transmitter was close to the boundary endpoints, the efficiency
809 was very poor. And the anisotropy couldn't be solved. These two points had yet to be
810 further studied.

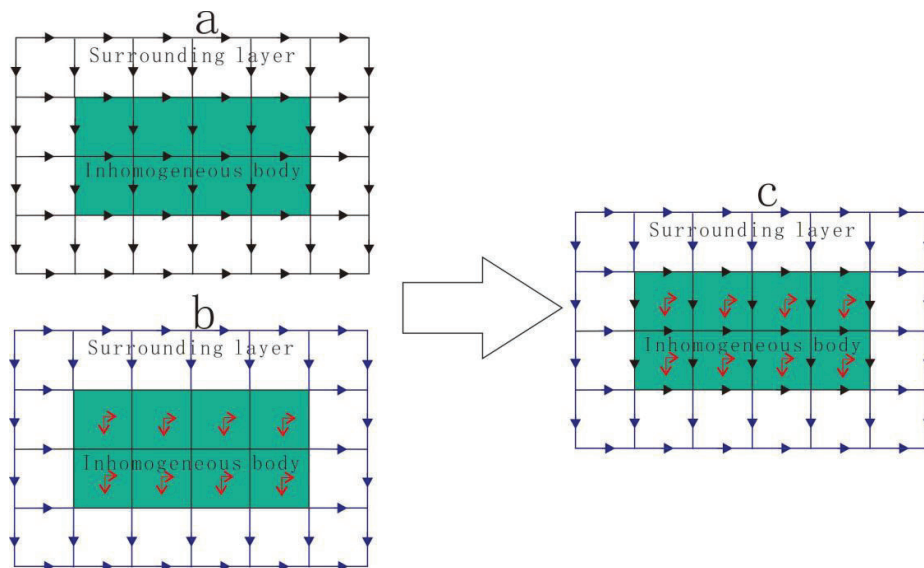
811 On the whole, IE is very useful for 3D EM fields simulation. Although its
812 applicability is not as extensive as FEM and FD, it only meshes the scattering
813 anomaly region, which greatly reduces the number of meshes compared with FEM
814 and FD meshing in the whole half space. It reduces the calculation of the unknowns,
815 so that there is a clear advantage in the calculation speed. In addition, since converting
816 the Maxwell's differential equations into the form of the integral equations, in
817 principle, IE has a characteristic of semi-analytical solution, and the solution accuracy
818 is not affected too much by the meshing. However, IE is difficult to handle the
819 complex anisotropy and non-horizontal layered background media but FEM and FD
820 are more suitable for such issues. Moreover, due to the heavy limitation to the
821 accuracy of solving linear equations, most EM software developers avoid using the IE
822 method (Avdeev, 2005). Therefore, taking advantages and drawbacks of these,
823 coupling IE and FEM or FD to form a new hybrid scheme, it can better achieve a
824 relatively balance between the accuracy and the efficiency of forward modeling.

825 **2.4 Hybrid methods**

826 With the further development of FEM, FD and IE, for more complex models and
827 a larger amount of data, a single forward modeling method is not enough for more
828 accurate and efficient simulation. Some hybrid schemes which combined the
829 characteristics and advantages of several methods has been developed.

830 **2.4.1 The solutions to calculate the field boundary**

831 It is well-known that edge-based FEM (or vector FEM) is widely used to solve
832 the Maxwell's differential equations about the secondary electric fields, however, the
833 approximation on the field boundaries is limited to computational domain. In order to
834 resolve such boundary restriction, Ren et al. (2014b) proposed a hybrid
835 boundary-element finite-element method (BEM-FEM) for goal-oriented adaptive
836 multi-level fast algorithm to simulate the 3D EM induction response of plane waves.
837 This method, which coupled the Galerkin vector FEM (Jin, 2002) method with the
838 point collocation boundary-element method, had the ability to simulate the problems
839 of the large-scale complex earth EM induction, and it was better than the conventional
840 FEM method at high frequency. Differently from the method combined FEM and
841 BEM, Liu et al. (2018a) applied IE method to calculate the boundary values by
842 solving the Green's functions. They developed a hybrid solver based on IE and
843 boundary-based vector FEM to simulate 3D CSEM model. They applied the vector
844 FEM to solve Maxwell's differential equation, and calculated the secondary electric
845 field at the receivers by IE, as Figure 6 showed. A more accurate and efficient solution
846 for high conductivity contrast medium was obtained compared to the traditional
847 method.



848
849 Figure 6. Plane view of the evolution process of the hybrid grid, from the vector FEM
850 and IE grids. (a) The vector FEM grid with electric fields (black arrow lines) defined
851 on grid edges; (b) IE grid with scattering currents (red arrow lines) defined at the

1 852 center of inner cells (green color), and boundary electric fields (blue arrow lines)
2 853 located at the edges of boundary cells (white color); and (c) in the hybrid scheme, the
3 854 boundary electric fields are given in terms of scattering currents by IE; the scattering
4 855 current within each cell in turn can be represented by electric fields (black arrow lines)
5 856 within the cell using the edge-shape function of vector FEM (Liu et al. 2018a).

6 857 Nowadays, a coupling method of FEM and infinite element method (IFEM) is
7 858 still in a research stage in the field of geophysical EM method. IFEM was first
8 859 proposed by Bettess (1977a) mainly applied in the research of acoustics,
9 860 electromagnetism, geotechnical mechanics engineering, etc. In the same year, Bettess
10 861 (1977b) proposed the coupling method of FEM and IFEM. Fu and Wu (2000)
11 862 introduced IFEM into the geophysical field to deal with the boundary conditions of
12 863 absorbing elastic waves. IFEM overcame some of the difficulties encountered in
13 864 conventional absorption techniques, so that it took up less memory space and reduced
14 865 more computation time. The coupling between FEM and IFEM was achieved by
15 866 adding an infinite element outside the boundary of the finite element splitting unit and
16 867 then mapping it to infinity through coordinate mapping to achieve integration of
17 868 infinity and neglect the boundary condition. Although this hybrid scheme is not very
18 869 mature in the study of geophysical EM method, it has a good application prospect.

26 870 **2.4.2 The improvements of the computing accuracy and efficiency**

27
28 871 According to the foregoing, the linear system of IE is independent from grid
29 872 meshing but difficult to settle down the anisotropy. However, FD has the advantage of
30 873 high-discretization to make up for this deficiency. Based on this thinking, Zaslavsky
31 874 et al. (2011) proposed a hybrid finite-difference integral equation method (FDIE) for
32 875 CSEM, single-well and crosswell EM modeling, along with the complex structure and
33 876 anisotropy. The FDIE overcame the large condition number of the system of the
34 877 traditional FD and decreased size of the computation domain. The optimization
35 878 formed from combining with FD homogenization and optimal meshing algorithms
36 879 was suitable for discretization. In the same idea, Yoon et al. (2016) developed a new
37 880 hybrid 3D marine CSEM modeling method combining the advantages of FD and IE.
38 881 Something different from Zaslavsky et al. (2011), the precondition operator for FD
39 882 solver was replaced with the MUMPS direct solver. And SFD was used to solve the
40 883 Maxwell's equations in the electric field. The Green's tensor of the corresponding
41 884 background conductivity model was calculated by IE. The hybrid solution overcame
42 885 the problem of marine CSEM consuming a lot of time and memory in the case of
43 886 multiple transmitters and receivers.

44
45 887 As a conclusion, the hybrid scheme is more efficient and accurate than the
46 888 traditional single method. Compared with the traditional method, the hybrid scheme
47 889 can save more computation time and memory, and get a faster and more accurate
48 890 solution. However, there remains many difficulties in the technology of matching
49 891 hybrid scheme. Although the hybrid scheme is still in the research stage, considering
50 892 the wide applicability, the high efficiency and the value of these schemes, it will
51 893 become a main development trend of future EM forward modeling.

894 **2.5 Deep learning**

895 Artificial neural network (ANN) is a research hot spot that has emerged in the
896 field of artificial intelligence since the 1980s. ANN refers to a complex network
897 structure formed by a large number of processing units (neurons) connected to each
898 other. It is a certain abstraction, simplification and simulation of the human brain
899 tissue structure and operating mechanism and it has a strong ability to approximate
900 nonlinear functions. ANN has been applied in geophysical EM problems (Poulton et
901 al., 1992a, 1992b; Poulton & Birken 1998), such as well-log (Huang et al., 1996;
902 Zhang et al., 2002; Maiti and Tiwari, 2010), MT (Zhang and Paulson, 1997; Spichak
903 and Popova, 2000; Manoj and Nagarajan, 2003) and AEM (Seiberl, 1998; Ahl, 2003;
904 Andersen et al., 2016).

905 Deep learning (DL) can be simply understood as the development of ANN. The
906 concept of DL comes from the research of ANN. Through multi-layer processing,
907 after the initial low-level feature representation is gradually transformed into the
908 high-level feature representation with the high-dimensional data transforming into
909 low-dimensional, the simple models can be used to complete complex classification
910 and other learning tasks (Hinton and Salakhutdinov, 2006). The "deep" of deep
911 learning not only represents the depth of the multilayer neural network structure, but
912 also represents the deep extraction of feature information (LeCun et al., 2015).

913 The most typical deep learning model is convolutional neural network (CNN)
914 (LeCun et al., 1989) and CNN has been applied in geophysics EM imaging or
915 inversion due to the rapid development nowadays. Puzyrev (2019) used the DL
916 method for EM inversion based on fully CNN for 2.5D inversion and this is the first
917 application of deep CNN to EM inverse problems as we know. Inspired by this,
918 Moghadas (2020) proposed a new method of DL inversion based on CNN, which can
919 estimate the subsurface electrical conductivity layering from electromagnetic
920 induction data. Oh et al. (2019) successfully identified salt bodies from towed
921 streamer EM data with a CNN, and the prediction results demonstrated the
922 applicability of CNN for imaging resistivity from EM data. Haber et al. (2019) trained
923 a VNet CNN architecture to interpret 3D AEM inversions. For imaging subsurface
924 resistivity inversion from 1D AEM data in the frequency domain, Noh et al. (2020)
925 applied the deep neural network (DNN) method and the potential of DNNs for AEM
926 inversion interpretation was validated by comparison with the conventional
927 Gauss-Newton inversion algorithm. Similarly, Li et al. (2020) developed a new fast
928 imaging method of 1D AEM data in the time domain using a long short-term memory
929 (LSTM) DNN (Hochreiter and Schmidhuber, 1997). DL can also eliminate
930 multi-source noise of AEM data (Wu et al., 2020).

931 In addition, the training synthetic data generation process of the above deep
932 learning is still inseparable from the traditional forward modeling method to solve the
933 PDEs. Puzyrev (2019) used the parallel 3D SFD code based on the curl-curl electric
934 field formulation and Oh et al. (2019) adopted the 2.5D FEM method in the frequency
935 domain proposed by Kang et al. (2012). An efficient and accurate forward algorithm

936 will provide DL with more reliable training data to get more credible prediction
937 results.

938 Above all, since the method of establishing a nonlinear relationship and solving
939 the gradient is adopted, in a sense, the DL method is similar to inversion in a broad
940 sense. Compared with the iteration of traditional inversion, deep learning uses a
941 multi-layer feature extraction method to maximize the extraction of useful
942 information in the original data, without causing too much accuracy loss under the
943 interference of random noise. Unlike traditional inversion, which requires re-iterative
944 calculations for each inversion, a neural network model trained based on certain
945 research data has a certain degree of commonality for similar survey.

946 In fact, DL technology also has the potential to simulate the EM field not going
947 through the complex solution of Maxwell's equations. [Tang et al. \(2017\)](#) made an
948 investigation on it. They applied CNN into the simulation of 2D electrostatic problem
949 and the results of the study demonstrated the possibility and by building up a fast FD
950 solver the computing complexity was exactly reduced. In addition, [Khan et al. \(2019\)](#)
951 efficiently estimated the distribution of the magnetic field by using the DL field
952 estimator model learning from the finite-element analysis. Although there is still room
953 for improvement in the structure of the network, the study has reduced calculation
954 time cost and has the advantage of parallelization. [Shahriari et al. \(2020\)](#) examined
955 the potential of DNN that can replace the traditional PDE solution method for forward
956 simulation of borehole resistivity measurements. However, the paper also pointed out
957 that it requires a sufficiently large data set to produce a reasonably accurate forward
958 function and the application still faces many difficulties and challenges.

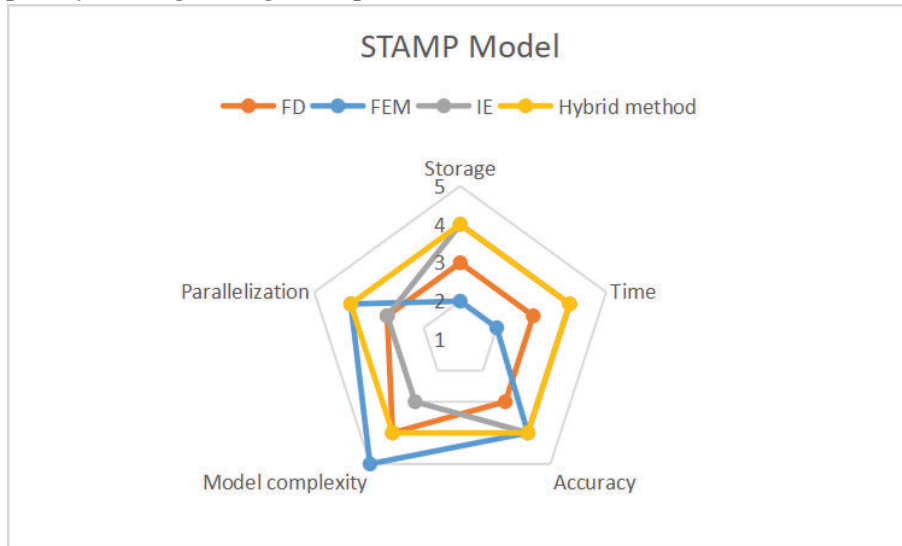
959 At present, there are very few related researches, exclusively in the exploratory
960 research stage. The existing data-driven DL forward modeling requires the use of
961 traditional forward solvers, such as FD ([Tang et al., 2017](#); [Shahriari et al., 2020](#)) or FE
962 ([Khan et al., 2019](#)), to make a training data set. The difference from DL "inversion" is
963 that DL "forward modeling" uses the EM models as the input of the neural network,
964 and the output is the responses. Therefore, for DL, there is no distinction between
965 forward and inverse problems, only training, validation and testing, and the
966 intermediate processes are similar. For neural networks, there is only the difference
967 between input and output, or known and unknown. In other words, it depends on what
968 kind of task we want to accomplish in order to achieve what kind of goal.

969 However, there are still two problems to be solved. One is that the essential
970 feature of DL is data-driven. The realization of DL is based on training with a large
971 amount of data. To a certain extent, the more training data, the more adequate the
972 training of the neural network, and then the more accurate prediction results will be.
973 How to obtain adequate training data or how to deal with the problem of insufficient
974 training due to inadequate sample size? The other is the applicability of network
975 model to EM modeling. What kind of network structure is more conducive to learning
976 and predicting the realistic EM field distribution? And for EM modeling, the
977 aforementioned DL methods for PDEs are all solutions to 1D or 2D problems, how to
978 achieve 3D modeling? Although DL methods seem to have become a hot spot for

979 geophysical applications in the past five years mentioned in Section 1, these issues
980 need to be further studied in the future.

981 3. Discussions

982 Based on the collation and summary of all corresponding references involved,
983 we put forward a Qualitative Evaluation Model named STAMP Model, which is
984 shown in Figure 7. Storage, time, accuracy, model complexity and parallelization
985 these five criteria are used to evaluate the advantages and disadvantages of the
986 forward modeling methods. We divided the five key criteria into five levels from 1 to
987 5. When the value of level is higher, they respectively represent less computing
988 memory, shorter computing time, higher calculation accuracy, higher model
989 complexity and higher degree of parallelization.



990
991 Figure 7. STAMP Model for modeling evaluation.

992 FD is an efficient tool to solve the EM modeling with simple implementation
993 (Streich, 2009; Yavich and Zhdanov, 2016). It can handle the discontinuity of the
994 magnetic field and electric field caused by the electromagnetic difference in the
995 internal medium very well, because of the characteristics of the staggered grid (Yee,
996 1966; Smith, 1996a). However, the regular structure mesh of the model restricts the
997 application of FD in complex geophysical models, which also affects its calculation
998 accuracy (Key and Weiss, 2006; Key and Oval, 2011).

999 FEM is the most flexible for simulating complex and large-scale geometry
1000 models with high computation accuracy (Avdeev, 2005; Börner, 2010). However, The
1001 number of unknowns is often on the order of millions and it performs with higher
1002 computer memory and computational cost (Puzyrev et al., 2013; Ren et al., 2014a).
1003 The flexibility of unstructured grids, such as tetrahedral or hexahedral grid, improves
1004 the calculation accuracy of complex geoelectric structures to a certain extent. The
1005 accuracy of the finite element depends on the size of the element and the order of the
1006 shape function (Jin, 2002). Unfortunately, it still lacks the analytic solutions to 3D

1007 problems (Smith, 1996a).

1008 IE is suitable for simple 3D models in a layered earth, which only needs to
1009 discretize the computational area within the range of the scattering anomaly resulting
1010 in small system matrices, so that it takes up less computing memory and has higher
1011 efficiency (Hohmann, 1971; Avdeev et al., 2002). Due to the numerical results of IE
1012 have the accuracy of a semi-analytical solution, IE is often used to test the accuracy of
1013 newly developed algorithms (Ren and Tang, 2010). However, as the size of the model
1014 becomes larger and the complexity increases, the computational efficiency of IE will
1015 be greatly reduced (Mackie et al., 1994). And the accuracy of the solution is heavily
1016 dependent on the accuracy of the complicated and time-consuming system matrix
1017 which is an extremely tedious and nontrivial problem itself (Avdeev, 2005). These
1018 drawbacks limit the solution of IE to solve complex EM models, especially the
1019 complex, high-contrast inhomogeneous anisotropic medium (Zaslavsky et al., 2011).

1020 Hybrid method has the advantage to solve some special problems, because it
1021 combines the advantages from different modeling methods. Hybrid methods are
1022 indeed effective strategies for improvements (Zaslavsky et al., 2011; Ren et al., 2014b;
1023 Yoon et al., 2016; Liu et al., 2018a). Given that, in our STAMP Model, the hybrid
1024 method maybe has a balance between accuracy and efficiency.

1025 It is important to point out that for the criteria of parallelization, the specific
1026 situation requires specific analysis, such as utilizing a direct solver or iterative solver
1027 and computing by single-core or multi-core processing cards. It depends on the
1028 models of parallelization such as shared memory or distributed memory and
1029 multithreading or multiprocessing. So, it is very difficult to quantitatively analyze the
1030 degree of parallelization of FD, FEM and IE. However, from the perspective of the
1031 algorithm itself, FEM is suitable for complex and large-scale models and has the
1032 characteristics of high accuracy but large memory usage and time-consuming
1033 calculations. In this case, the parallelization scheme is more conducive to the balance
1034 of high precision and high efficiency. In addition, according to the literature citations
1035 in this review, researchers indeed have more research on parallel FEM than FD or IE.
1036 Therefore, a qualitative comparison was given that the degree of the parallelization of
1037 FEM is higher than FD and IE.

1038 DL is not included in the STAMP model for comparison with other methods,
1039 because the current researches are not enough to explain its advantages and
1040 disadvantages with traditional forward modeling methods in geophysical EM. As far
1041 as we know, in modern deep learning, the number of parameters is increasing, and the
1042 data sets are getting larger, so that it is difficult to load all the data sets into the
1043 memory. To train a complex deep learning model on a larger data set, machine
1044 learning on a single node takes too long, and multi-node parallel computing has to be
1045 used. Furthermore, according to the current research situation, the introduced DL
1046 method may provide high speed to compute the model. The complexity of the training
1047 model and the accuracy of the prediction model need to be improved.

1 1048 **4. Conclusions**

2
3
4
5 1049 In this paper, we review the mainly simulation method in EM field modeling.
6 1050 Three most widely employed methods in EM modeling include FEM, FD and IE
7 1051 method. Based on the published 195 papers, we summarized the advantages and
8 1052 disadvantages of these modeling methods. It is complex to judge which is the best
9 1053 modeling method, due to different applications. So, we proposed the STAMP Model
10 1054 for qualitative evaluations of FD, FEM, IE, and hybrid methods. We also reviewed
11 1055 and discussed the application of DL in geophysical EM forward and inversion
12 1056 problems.

13 1057 Above all, the EM field simulation methods have been developed to solve the
14 1058 different problems in high-dimensional, complex geometry model, high accuracy,
15 1059 high computational speed. And in the future, the EM modeling research will focus on
16 1060 the high accuracy and low computational cost solutions in large-scale,
17 1061 high-dimensional and anisotropic medium combining HPC and artificial intelligence.

18
19
20
21
22
23
24
25 1062 **Acknowledgement**

26
27
28
29 1063 This research is supported by Basic Science Center Project for National Natural
30 1064 Science Foundation of China (No. 72088101, the Theory and Application of Resource
31 1065 and Environment Management in the Digital Economy Era), and it has also been
32 1066 supported by the Natural Science Foundation of China (NSFC) (41804073;
33 1067 42074171). It is supported by Changsha Municipal Natural Science Foundation
34 1068 (kq2014124). Furthermore, the research got the Grant from the Open Foundation of
35 1069 Key Laboratory of Submarine Geosciences, SOA(KLSG1905). This work was
36 1070 supported in part by Hunan Provincial Natural Science Foundation of China (Grant:
37 1071 2019JJ40371)

38 1072
39 1073 Data availability Statement: 'Not Applicable'.

40 1074 This review includes the number of the EM publication could be found by Google.

41
42
43
44
45
46
47
48 1075 **Appendix A**

49
50
51
52 1076 Finite difference solution of Maxwell equations: taking the MT for the isotropic
53 1077 media as an example

54
55
56 1078 First, we discrete the research area. A series of parallel planes are used to divide
57 1079 the research area into several small rectangular cells at different distances along the X,
58 1080 Y, and Z axis directions. Assuming that they are divided into N_x , N_y , and N_z segments
59 1081 along the X, Y, and Z axis directions, respectively.

60
61
62
63
64
65

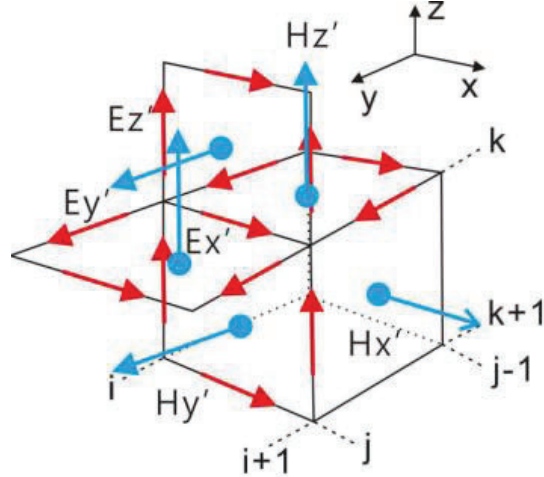


Figure 8. The staggered grid.

We use the staggered grid in Figure 2 (a). Figure 8 shows the grid element numbered (i, j, k) . The value of resistivity is $\rho(i, j, k)$. Its length, width and height are respectively Δx_i ($i = 1, 2, \dots, N_x$), Δy_j ($j = 1, 2, \dots, N_y$) and Δz ($k = 1, 2, \dots, N_z$). And we define E_x' , E_y' , E_z' as the average value of the electric field at the central point of the edge of the grid cell; H_x' , H_y' , H_z' respectively represent the average value of the magnetic field at the central point of the plane of the grid cell.

According to the theory of the MT method, under the quasi-static condition, the integral form of Maxwell's equations in the frequency domain is as follows.

$$\begin{aligned}
 \oint_l \mathbf{E} dl &= i\omega\mu \iint_s \mathbf{H} dS, \\
 \oint_l \mathbf{H} dl &= \iint_s \sigma \mathbf{E} dS, \\
 \oint_l \mathbf{H} dS &= 0, \\
 \oint_l \mathbf{E} dS &= 0,
 \end{aligned} \tag{1}$$

Where \mathbf{E} is the electric field strength, \mathbf{H} is the magnetic field strength, σ is the conductivity, i is the imaginary unit, ω is the circular frequency, μ is the permeability of underground media, dl is the enclosure line of the enclosed integration, and dS is the area contained in the enclosure line.

Discretization of equation (1) can be obtained as follows. μ is approximated to μ_0 ($= 4\pi \times 10^{-7} \text{ H/m}$), which is the magnetic permeability for free space.

$$\begin{aligned}
& \left[E_z(i, j, k) - E_z(i, j-1, k) \right] \bullet \frac{\Delta z_{k-1} + \Delta z_k}{2} - \left[E_y(i, j, k) - E_y(i, j, k-1) \right] \bullet \frac{\Delta y_{j-1} + \Delta y_j}{2} \\
& = i\mu_0 \omega H_x(i, j, k) \bullet \frac{\Delta z_{k-1} + \Delta z_k}{2} \bullet \frac{\Delta y_{j-1} + \Delta y_j}{2}, \\
& \left[E_x(i, j, k) - E_x(i, j, k-1) \right] \bullet \frac{\Delta x_{i-1} + \Delta x_i}{2} - \left[E_z(i, j, k) - E_z(i-1, j, k) \right] \bullet \frac{\Delta z_{k-1} + \Delta z_k}{2} \\
& = i\mu_0 \omega H_y(i, j, k) \bullet \frac{\Delta x_{i-1} + \Delta x_i}{2} \bullet \frac{\Delta z_{k-1} + \Delta z_k}{2}, \\
& \left[E_y(i, j, k) - E_y(i-1, j, k) \right] \bullet \frac{\Delta y_{j-1} + \Delta y_j}{2} - \left[E_x(i, j, k) - E_x(i, j-1, k) \right] \bullet \frac{\Delta x_{i-1} + \Delta x_i}{2} \\
& = i\mu_0 \omega H_z(i, j, k) \bullet \frac{\Delta x_{i-1} + \Delta x_i}{2} \bullet \frac{\Delta y_{j-1} + \Delta y_j}{2}, \\
& \left[H_z(i, j+1, k) - H_z(i, j, k) \right] \bullet \Delta z_k - \left[H_y(i, j, k+1) - H_y(i, j, k) \right] \bullet \Delta y_j = \sigma_x(i, j, k) E_x(i, j, k) \bullet \Delta y_j \bullet \Delta z_k, \\
& \left[H_x(i, j, k+1) - H_x(i, j, k) \right] \bullet \Delta x_i - \left[H_z(i+1, j, k) - H_z(i, j, k) \right] \bullet \Delta z_k = \sigma_y(i, j, k) E_y(i, j, k) \bullet \Delta x_i \bullet \Delta z_k, \\
& \left[H_y(i+1, j, k) - H_y(i, j, k) \right] \bullet \Delta y_j - \left[H_x(i, j+1, k) - H_x(i, j, k) \right] \bullet \Delta x_i = \sigma_z(i, j, k) E_z(i, j, k) \bullet \Delta x_i \bullet \Delta y_j,
\end{aligned} \tag{2}$$

Where σ_x , σ_y , σ_z are respectively the conductivities in X, Y and Z directions. The expressions are as follows.

$$\begin{cases}
\sigma_x(i, j, k) = \frac{1}{\rho_x(i, j, k)} = \frac{\Delta x_i + \Delta x_{i-1}}{\rho(i, j, k)\Delta x_i + \rho(i-1, j, k)\Delta x_{i-1}}, \\
\sigma_y(i, j, k) = \frac{1}{\rho_y(i, j, k)} = \frac{\Delta y_j + \Delta y_{j-1}}{\rho(i, j, k)\Delta y_j + \rho(i, j-1, k)\Delta y_{j-1}}, \\
\sigma_z(i, j, k) = \frac{1}{\rho_z(i, j, k)} = \frac{\Delta z_k + \Delta z_{k-1}}{\rho(i, j, k)\Delta z_k + \rho(i, j, k-1)\Delta z_{k-1}},
\end{cases} \tag{4}$$

After simultaneous polynomials and elimination, the system of linear equations for the electric field component or the magnetic field component can be obtained as follows.

$$\mathbf{Ax} = \mathbf{b}$$

Then, we can solve the system of linear equations by using various methods, including direct solver, LU decomposition, the Krylov subspace iterative solution and so on.

Appendix B

Finite element solution of Maxwell equations: taking the the electric field of MT for the isotropic media as an example

According to the theory of the MT method, under the quasi-static condition, the differential form of Maxwell's equations in the frequency domain is as follows.

1
2
3 1116
4
5
6
7

$$\begin{cases} \nabla \times \mathbf{E} = -i\omega\mu\mathbf{H}, \\ \nabla \times \mathbf{H} = \sigma\mathbf{E}, \\ \nabla \cdot \mathbf{H} = 0, \\ \nabla \cdot \mathbf{E} = 0, \end{cases} \quad (5)$$

8 1117 Where \mathbf{E} is the electric field strength, \mathbf{H} is the magnetic field strength, σ is the
9 1118 conductivity, i is the imaginary unit, ω is the circular frequency, and μ is the
10 1119 permeability of underground media.

11 1120 We simultaneously calculate the curl of both sides of the first formula in the
12 1121 system of equation (5), and combining the second formula, the solution can be
13 1122 obtained as follows.

14 1123
$$\nabla \times \nabla \times \mathbf{E} + i\omega\mu_0\sigma\mathbf{E} = 0 \quad (6)$$

15 1124 We use Galerkin method (Jin, 2002) to derive the system of equation (6).
16 1125 And we use the simple Dirichlet boundary conditions (Nam et al., 2007).

17 1126
$$\mathbf{E} \times \mathbf{n} = \mathbf{E}_o \times \mathbf{n} \quad (7)$$

18 1127 Where \mathbf{n} is the outer unit normal vector of the outer boundary, \mathbf{E}_o is the given
19 1128 known electric field strength on the outer boundary

20 1129 Equations (6) and (7) are the boundary value problems for MT forward modeling.

21 1130 Using the vector formula $\mathbf{B} \cdot (\nabla \times \mathbf{A}) = \mathbf{A} \cdot (\nabla \times \mathbf{B}) + \nabla \cdot (\mathbf{A} \times \mathbf{B})$ and Green's integral
22 1131 equation (Nam et al., 2007), we obtain the corresponding variation expression by
23 1132 combing equation (6) and (7).

24 1133
$$b(\mathbf{E}, \mathbf{V}) = f(\mathbf{V}), \mathbf{V} \in H(\text{curl}) \quad (8)$$

25 1134 Where $H(\text{curl}) = \{\mathbf{V} \mid \mathbf{V} \in L_2(\Omega), \mathbf{V} \times \mathbf{n} = \mathbf{n} \times \mathbf{V}_o\}$, $L_2(\Omega)$ is the second-order
26 1135 derivative continuous function space, \mathbf{n} is the unit normal vector on outer boundary, b
27 1136 and f are expressed as:

28 1137
$$b = \int_{\Omega} (\nabla \times \mathbf{E} \cdot \nabla \times \mathbf{V} - i\omega\mu\sigma\mathbf{E} \cdot \mathbf{V}) d\Omega \quad (9)$$

29 1138
$$f = \int_{\partial\Omega} \mathbf{V} \cdot \mathbf{E}_o d\Gamma \quad (10)$$

30 1139 We use the vector FEM to solve the electric field distribution represented by
31 1140 equation (6) and use unstructured tetrahedral element grid for spatial discretization.
32 1141 The numbering rules of the edges of the tetrahedral elements are shown in the Figure
33 1142 9.

34
35
36
37
38
39
40
41
42
43
44
45
46
47
48
49
50
51
52
53
54
55
56
57
58
59
60
61
62
63
64
65

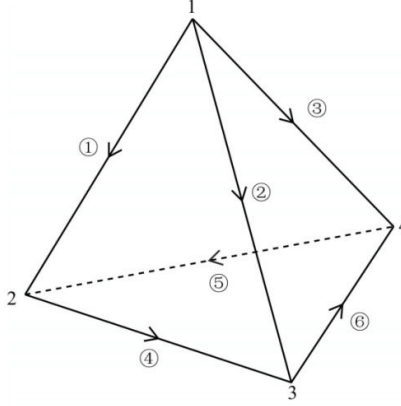


Figure 9. Edge definition of tetrahedral element.

For any tetrahedral element e , approximate expression of the electric field in this element is as follows.

$$\mathbf{E}^e = \sum_{i=1}^n \mathbf{N}_i^e E_i^e \quad (11)$$

Where $n=6$, which is the numbers of edge in each element, E_i is the tangential electric field on the i th edge of the i th element, and \mathbf{N}_i is the vector shape function on the i th edge of the i th element (Jin, 2002). We designate the i th edge vector shape function as:

$$N_i^e = l_i^e (L_{i1}^e \nabla L_{i2}^e - L_{i2}^e \nabla L_{i1}^e) \quad (12)$$

where l_i^e is the length of i th edge. L_{i1}^e and L_{i2}^e are the origin node shape functions defined at each node of the i th edge.

Then, substituting the equation (11) and (12) into the equation (9), we can get a large complex linear matrix equation

$$\mathbf{K}\mathbf{U} = \mathbf{F}$$

Where \mathbf{K} is a stiffness matrix, which reflects the topological relationship between grid nodes, \mathbf{U} is a matrix of electric field vectors to be calculate at all nodes and \mathbf{F} is a mass matrix and only the edge on the outer Dirichlet boundary is not zero. \mathbf{K} and \mathbf{F} can be:

$$\begin{aligned} K_{ij}^e &= \int_{\Omega^e} \nabla \times N_i \cdot \nabla \times N_j - i\omega\mu\sigma N_i N_j d\Omega \\ F_{ij}^e &= \int_{\partial L^e} N_i \cdot E_o d\Gamma \end{aligned} \quad (13)$$

Appendix C

Integral equation solution of Maxwell equations: taking the the electric field of MT for the isotropic media as an example

1167 According to the EM theory, the EM field at any point in the model can be
 1168 expressed as the superposition of the incident fields \mathbf{E}_i (\mathbf{H}_i) and scattered fields \mathbf{E}_s
 1169 (\mathbf{H}_s)

$$1170 \quad \begin{cases} \mathbf{E} = \mathbf{E}_i + \mathbf{E}_s \\ \mathbf{H} = \mathbf{H}_i + \mathbf{H}_s \end{cases} \quad (14)$$

1171 The incident field is generated by the incident source in the layered ground,
 1172 while the scattered field is caused by the difference in conductivity $\Delta\sigma = \sigma_b - \sigma_s$
 1173 between the anomalous body and the layered ground.

1174 According to the Green's Function Theory (Ting and Hohmann, 1981;
 1175 Wannamaker et al., 1984), the scattering field \mathbf{E}_s can be written as

$$1176 \quad \mathbf{E}_s(\mathbf{r}) = \iiint_{\Omega} \mathbf{G}^{JE}(\mathbf{r}, \mathbf{r}') \cdot \Delta\sigma(\mathbf{r}') \cdot \mathbf{E}(\mathbf{r}') dV \quad (10)$$

1177 Where \mathbf{G}^{JE} is the Green's Function of the electric field, Ω is the area where the
 1178 anomaly is located. Substituting the equation (10) into the the first formula in the
 1179 system of equation (9), we can obtain

$$1180 \quad \mathbf{E}(\mathbf{r}) = \mathbf{E}_i(\mathbf{r}) + \iiint_{\Omega} \mathbf{G}^{JE} \cdot \Delta\sigma(\mathbf{r}') \cdot \mathbf{E}(\mathbf{r}') dV$$

1181 We discretized the anomalous body into several small volume units Ω_i ($i = 1,$
 1182 $2, \dots, N$). Assuming that the electric field and conductivity in each cell are constant
 1183 and equal to the value of the cell center \mathbf{r}_i , we can get a discretized matrix equation

$$1184 \quad \mathbf{A} \cdot \mathbf{E} = \mathbf{E}_i \quad (11)$$

1185 Where $\mathbf{E} = [\mathbf{E}(\mathbf{r}_1), \mathbf{E}(\mathbf{r}_2), \dots, \mathbf{E}(\mathbf{r}_M)]^T$ and $\mathbf{E}_i = [\mathbf{E}_i(\mathbf{r}_1), \mathbf{E}_i(\mathbf{r}_2), \dots, \mathbf{E}_i(\mathbf{r}_M)]^T$ are
 1186 respectively the $3M$ order vectors consisting of the unknown electric field and the
 1187 incident electric field at the midpoint of each discrete unit. \mathbf{A} is a $3M \times 3M$ square
 1188 matrix, whose elements are composed of the following series of 3×3 sub-matrices

$$1189 \quad A_{\alpha\beta} = I\delta_{\alpha\beta} - \Delta\sigma(\mathbf{r}_\beta) \cdot \iiint_{\Omega_\beta} G^{JE}(\mathbf{r}_\alpha, \mathbf{r}') dV$$

1190 Where $\alpha, \beta = 1, 2, \dots, M$ and $\delta_{\alpha\beta} = \begin{cases} 1, & \alpha = \beta \\ 0, & \alpha \neq \beta \end{cases}$. Solving the equation (11) can get the

1191 electric field on each discrete element of the anomaly and then substituting the
 1192 solution into equation (10), the scattered field distribution at any position in space can
 1193 be obtained.

1194 Reference

1195 Abubakar, A., Habashy, T., Druskin, V., Alumbaugh, D., Zerelli, A., Knizhnerman, L.,
 1196 (2006a). Two-and-half-dimensional forward and inverse modeling for marine
 1197 CSEM problems. SEG Technical Program Expanded Abstracts 2006. pp.

- 1198 750-754.
- 1 1199 Abubakar, A., van Den Berg, P. M., & Habashy, T. M. (2006b). An integral equation
2 approach for 2.5-dimensional forward and inverse electromagnetic scattering.
3 1200 Geophysical Journal International, 165(3), 744-762.
4 1201
- 5 1202 Abubakar, A. , Habashy, T. M. , Druskin, V. L. , Knizhnerman, L. , & Alumbaugh, D. .
6 (2008). 2.5 d forward and inverse modeling for interpreting low-frequency
7 1203 electromagnetic measurements. Geophysics, 73(4), F165-F177.
8 1204
- 9 1205 Ahl, A. (2010). Automatic 1D inversion of multifrequency airborne electromagnetic
10 1206 data with artificial neural networks: discussion and a case study. Geophysical
11 1207 Prospecting, 51(2), 89-98.
- 12 1208 Alumbaugh, D. L., Newman, G. A., Prevost, L., & Shadid, J. N. (1996). Three-
13 dimensional wideband electromagnetic modeling on massively parallel
14 1209 computers. Radio Science, 31(1), 1-23.
15 1210
- 16 1211 Andersen, K. K., Kirkegaard, C., Foged, N., Christiansen, A. V. and Auken, E. (2016).
17 Artificial neural networks for removal of couplings in airborne transient
18 1212 electromagnetic data: Geophysical Prospecting, 64, 741-752.
19 1213
- 20 1214 Amestoy, P. R., Duff, I. S., L'Excellent, T. Y. and Koster, J. (2000). MUMPS: A
21 1215 general purpose distributed memory sparse solver: Lecture Notes in Computer
22 1216 Science, 121-130.
- 23 1217 Ansari, S., & Farquharson, C. G. (2014). 3D finite-element forward modeling of
24 1218 electromagnetic data using vector and scalar potentials and unstructured grids.
25 1219 Geophysics, 79(4), E149-E165.
- 26 1220 Ansari, S. M., Farquharson, C. G., & MacLachlan, S. P. (2017). A gauged
27 1221 finite-element potential formulation for accurate inductive and galvanic
28 1222 modelling of 3-D electromagnetic problems. Geophysical Journal International,
29 1223 210(1), 105-129.
- 30 1224 Avdeev, D. B., Kuvshinov, A. V., Pankratov, O. V., & Newman, G. A. (1997).
31 1225 High-performance three-dimensional electromagnetic modelling using modified
32 1226 Neumann series. Wide-band numerical solution and examples. Journal of
33 1227 geomagnetism and geoelectricity, 49(11-12), 1519-1539.
- 34 1228 Avdeev, D. B., Kuvshinov, A. V., Pankratov, O. V., & Newman, G. A. (1998).
35 1229 Three-dimensional frequency-domain modeling of airborne electromagnetic
36 1230 responses. Exploration Geophysics, 29(1-2), 111-119.
- 37 1231 Avdeev, D. B., Kuvshinov, A. V., Pankratov, O. V., & Newman, G. A. (2002).
38 1232 Three-dimensional induction logging problems, Part I: An integral equation
39 1233 solution and model comparisons. Geophysics, 67(2), 413-426.
- 40 1234 Avdeev, D. B. (2005). Three-dimensional electromagnetic modelling and inversion
41 1235 from theory to application. Surveys in Geophysics, 26(6), 767-799.
- 42 1236 Avdeev, D., & Knizhnik, S. (2009). 3D integral equation modeling with a linear
43 1237 dependence on dimensions. Geophysics, 74(5), F89-F94.
- 44 1238 Badea, E.A., Everett, M.E., Newman, G.A. & Biro, O. (2001). Finite-element analysis
45 1239 of controlled-source electromagnetic induction using Coulomb gauged potentials,
46 1240 Geophysics, 66(3), 786-799.
- 47 1241 Baker, G.A., Graves-Morris, P.R. (1996). Padé Approximants. Cambridge University
48
49
50
51
52
53
54
55
56
57
58
59
60
61
62
63
64
65

1242 Press, New York.

1 1243 Berenger, J. P. (1994). A perfectly matched layer for the absorption of electromagnetic
2 waves. *Journal of computational physics*, 114(2), 185-200.

3 1244

4 1245 Bettess, P. (1977a). Infinite elements. *International Journal for numerical methods in*
5 *engineering*, 11(1), 53-64.

6 1246

7 1247 Bettess, P., & Zienkiewicz, O. C. (1977b). Diffraction and refraction of surface waves
8 using finite and infinite elements. *International Journal for Numerical Methods*
9 *in Engineering*, 11(8), 1271-1290.

10 1249

11 1250 Börner, R. U., Ernst, O.G., Spitzer, K. (2008). Fast 3-D simulation of transient
12 electromagnetic fields by model reduction in the frequency domain using Krylov
13 subspace projection. *Geophysical Journal International*, 173:766-780.

14 1252

15 1253 Börner, R. U. (2010). Numerical modelling in geo-electromagnetics: advances and
16 challenges. *Surveys in Geophysics*, 31(2), 225-245.

17 1254

18 1255 Cai, H., Xiong, B., Han, M., & Zhdanov, M. (2014). 3D controlled-source
19 electromagnetic modeling in anisotropic medium using edge-based finite element
20 method. *Computers & Geosciences*, 73, 164-176.

21 1257

22 1258 Cai, H., Hu, X., Li, J., Endo, M., & Xiong, B. (2017a). Parallelized 3D CSEM
23 modeling using edge-based finite element with total field formulation and
24 unstructured mesh. *Computers & Geosciences*, 99, 125-134.

25 1260

26 1261 Cai, H., Hu, X., Xiong, B., Auken, E., Han, M., & Li, J. (2017b). Finite element time
27 domain modeling of controlled-Source electromagnetic data with a hybrid
28 boundary condition. *Journal of Applied Geophysics*, 145, 133-143.

29 1263

30 1264 Cai, H., Hu, X., Xiong, B., & Zhdanov, M. S. (2017c). Finite-element time-domain
31 modeling of electromagnetic data in general dispersive medium using adaptive
32 Padé series. *Computers & Geosciences*, 109, 194-205.

33 1266

34 1267 Castillo Reyes, O., Puente, J. D. L., Modesto, D., Puzyrev, V., & Cela, J. M. (2016). A
35 Parallel Tool for Numerical Approximation of 3D Electromagnetic Surveys in
36 Geophysics. *Computación y Sistemas*, 20(1), 29-39.

37 1269

38 1270 Castillo-Reyes, O., de la Puente, J., & Cela, J. M. (2018). PETGEM: A parallel code
39 for 3D CSEM forward modeling using edge finite elements. *Computers &*
40 *geosciences*, 119, 123-136.

41 1272

42 1273 Chen, Y. H., Omeragic, D., Druskin, V., Kuo, C. H., Habashy, T., Abubakar, A.,
43 Knizhnerman, L. (2011). 2.5D FD modeling of EM directional propagation tools
44 in high-angle and horizontal wells. *SEG Technical Program Expanded Abstracts*
45 *2011. Society of Exploration Geophysicists.*, pp. 422-426.

46 1275

47 1276

48 1277 Cherevatova, M., Egbert, G. D., & Smirnov, M. Y. (2018). A multi-resolution
49 approach to electromagnetic modelling. *Geophysical Journal International*,
50 *214(1)*, 656-671.

51 1279

52 1280 Chew, W. C., & Weedon, W. H. (1994). A 3D perfectly matched medium from
53 modified Maxwell's equations with stretched coordinates. *Microwave and*
54 *optical technology letters*, 7(13), 599-604.

55 1282

56 1283 Chung, Y., Son, J. S., Lee, T. J., Kim, H. J., & Shin, C. (2014). Three-dimensional
57 modelling of controlled-source electromagnetic surveys using an edge
58 finite-element method with a direct solver. *Geophysical Prospecting*, 62(6),
59 1285

60

61

62

63

64

65

- 1286 1468-1483.
- 1 1287 Coggon, J. H. (1971). Electromagnetic and electrical modeling by the finite element
2 method. *Geophysics*, 36(1), 132-155.
- 3 1288
- 4 1289 Commer, M., & Newman, G. (2004). A parallel finite-difference approach for 3D
5 transient electromagnetic modeling with galvanic sources. *Geophysics*, 69(5),
6 1192-1202.
- 7 1291
- 8 1292 Courant, R., & Robbins, H. (1942). What is Mathematics?. *Bull. Amer. Math. Soc*, 48,
9 810-812.
- 10 1293
- 11 1294 Čuma, M., Gribenko, A., & Zhdanov, M. S. (2017). Inversion of magnetotelluric data
12 using integral equation approach with variable sensitivity domain: Application to
13 EarthScope MT data. *Physics of the Earth and Planetary Interiors*, 270, 113-127.
- 14 1296
- 15 1297 da Silva, N. V., Morgan, J. V., MacGregor, L., & Warner, M. (2012). A finite element
16 multifrontal method for 3D CSEM modeling in the frequency domain.
17 *Geophysics*, 77(2), E101-E115.
- 18 1299
- 19 1300 Davis, T. A., and Duff, I. S. (1997). An unsymmetric pattern multifrontal method for
20 sparse LU factorization: *SIAM Journal on Matrix Analysis and Applications*, 18,
21 1301 140-158.
- 22 1302
- 23 1303 Davydycheva, S., and Druskin, V (1999). Staggered grid for Maxwell's equations in
24 arbitrary 3D inhomogeneous anisotropic media, in Oristaglio, M. and Spies, B.,
25 Eds., *three-dimensional Electromagnetics: Soc. Expl. Geophys.*, 138-145.
- 26 1305
- 27 1306 Davydycheva, S., Druskin, V., & Habashy, T. (2003). An efficient finite-difference
28 scheme for electromagnetic logging in 3D anisotropic inhomogeneous media
29 *Finite-difference Scheme in Anisotropic Media. Geophysics*, 68(5), 1525-1536.
- 30 1308
- 31 1309 Debroux, P. S. (1996). 3D Modelling of the electromagnetic response of geophysical
32 targets using the FDTD method 1. *Geophysical prospecting*, 44(3), 457-468.
- 33 1310
- 34 1311 de la Kethulle de Ryhove, S., & Mittet, R. (2014). 3D marine magnetotelluric
35 modeling and inversion with the finite-difference time-domain method.
36 *Geophysics*, 79(6), E269-E286.
- 37 1313
- 38 1314 Du Fort, E., & Frankel, S. P. (1953). Stability conditions in the numerical treatment of
39 parabolic differential equations. *Mathematical Tables and other aids to
40 computation*, 7(43), 135-152.
- 41 1316
- 42 1317 Dunham, M. W., Ansari, S., & Farquharson, C. G. (2018). Application of 3D marine
43 controlled-source electromagnetic finite-element forward modeling to
44 hydrocarbon exploration in the Flemish Pass Basin offshore Newfoundland,
45 Canada. *Geophysics*, 83(2), WB33-WB49.
- 46 1319
- 47 1320
- 48 1321 Dyatlov, G., Onegova, E., & Dashevsky, Y. (2015). Efficient 2.5 D electromagnetic
49 modeling using boundary integral equations. *Geophysics*, 80(3), E163-E173.
- 50 1322
- 51 1323 Dyatlov, G., Kushnir, D., & Dashevsky, Y. (2017). Treatment of singularity in the
52 method of boundary integral equations for 2.5 D electromagnetic modeling.
53 *Geophysics*, 82(2), E57-E75.
- 54 1325
- 55 1326 Egbert, G. D., & Kelbert, A. (2012). Computational recipes for electromagnetic
56 inverse problems. *Geophysical Journal International*, 189(1), 251-267.
- 57 1327
- 58 1328 Everett, M., and Edwards, R. (1992). Transient marine electromagnetics: The 2.5-D
59 forward problem: *Geophysical Journal International*, 113, 545-561.
- 60 1329
- 61
- 62
- 63
- 64
- 65

- 1 1330 Fainberg, E. B., & Zinger, B. S. (1980). Electromagnetic induction in a non-uniform
2 1331 spherical model of the Earth. In *Annales de Geophysique* (Vol. 36, pp. 127-134).
- 3 1332 Farquharson, C. G., & Oldenburg, D. W. (2002). An integral equation solution to the
4 1333 geophysical electromagnetic forward-modelling problem. In *Methods in*
5 1334 *Geochemistry and Geophysics* (Vol. 35, pp. 3-19). Elsevier.
- 6 1335 Farquharson, C. G., Duckworth, K., & Oldenburg, D. W. (2006). Comparison of
7 1336 integral equation and physical scale modeling of the electromagnetic responses
8 1337 of models with large conductivity contrasts. *Geophysics*, 71(4), G169-G177.
- 9 1338 Farquharson, C. G., & Miensoopust, M. P. (2011). Three-dimensional finite-element
10 1339 modelling of magnetotelluric data with a divergence correction. *Journal of*
11 1340 *Applied Geophysics*, 75(4), 699-710.
- 12 1341 Fu, H., Wang, Y., Um, E. S., Fang, J., Wei, T., Huang, X., & Yang, G. (2015). A
13 1342 parallel finite-element time-domain method for transient electromagnetic
14 1343 simulation. *Geophysics*, 80(4), E213-E224.
- 15 1344 Fu, L. Y., & Wu, R. S. (2000). Infinite boundary element absorbing boundary for
16 1345 wave propagation simulations. *Geophysics*, 65(2), 596-602.
- 17 1346 Goldman, M. M., & Stoyer, C. H. (1983). Finite-difference calculations of the
18 1347 transient field of an axially symmetric earth for vertical magnetic dipole
19 1348 excitation. *Geophysics*, 48(7), 953-963.
- 20 1349 Grayver, A.V. & Burg, M. (2014). Robust and scalable 3-D geo-electromagnetic
21 1350 modelling approach using the finite element method, *Geophysical Journal*
22 1351 *International*, 198(1), 110-125.
- 23 1352 Grayver, A.V., Streich, R. & Ritter, O. (2013). Three-dimensional parallel distributed
24 1353 inversion of CSEM data using a direct forward solver, *Geophysical Journal*
25 1354 *International*, 193(3), 1432-1446.
- 26 1355 Grayver, A. V. (2015). Parallel three-dimensional magnetotelluric inversion using
27 1356 adaptive finite-element method. Part I: theory and synthetic study. *Geophysical*
28 1357 *Journal International*, 202(1), 584-603.
- 29 1358 Grayver, A. V., & Kolev, T. V. (2015). Large-scale 3D geoelectromagnetic modeling
30 1359 using parallel adaptive high-order finite element method EM modeling with
31 1360 high-order FEM. *Geophysics*, 80(6), E277-E291.
- 32 1361 Grayver, A. V., van Driel, M., & Kuvshinov, A. V. (2019). Three-dimensional
33 1362 magnetotelluric modelling in spherical Earth. *Geophysical Journal*
34 1363 *International*, 217(1), 532-557.
- 35 1364 Haber, E., Fohring, J., McMillan, M. & Granek, J. (2019) Using machine learning to
36 1365 interpret 3D airborne electromagnetic inversions, *ASEG Extended Abstracts*,
37 1366 2019:1, 1-4.
- 38 1367 Haynsworth, E. V. (1968). On the Schur complement: *Basel Mathematical Notes*,
39 1368 *University of Basel*, BMN 20.
- 40 1369 Heagy, L. J., Kang, S., Cockett, R., & Oldenburg, D. W. (2019). Open-source software
41 1370 for simulations and inversions of airborne electromagnetic data. *Exploration*
42 1371 *Geophysics*, 1-7.
- 43 1372 Hinton, G. E. and Salakhutdinov, R. R. (2006). Reducing the Dimensionality of Data
44 1373 with Neural Networks. *Science*, 313(5786), 504-507.
- 45
46
47
48
49
50
51
52
53
54
55
56
57
58
59
60
61
62
63
64
65

1374 Hochreiter, S., and J. Schmidhuber. (1997). Long short-term memory: Neural
1375 Computation, 9, 1735-1780.

1376 Hohmann, G. W. (1971). Electromagnetic scattering by conductors in the earth near a
1377 line source of current. *Geophysics*, 36(1), 101-131.

1378 Hohmann, G. W. (1975). Three-dimensional induced polarization and electromagnetic
1379 modeling. *Geophysics*, 40(2), 309-324.

1380 Hohmann, G. W. (1983). Three-dimensional EM modeling. *Geophysical Surveys*,
1381 6(1-2), 27-53.

1382 Hou, J., Mallan, R. K., & Torres-Verdín, C. (2006). Finite-difference simulation of
1383 borehole EM measurements in 3D anisotropic media using coupled scalar-vector
1384 potentials. *Geophysics*, 71(5), G225-G233.

1385 Huang, Z. , Shimeld, J. , Williamson, M. , & Katsube, J. . (1996). Permeability
1386 prediction with artificial neural network modeling in the venture gas field,
1387 offshore eastern canada. *Geophysics*, 61(2), 422-436.

1388 Hrennikoff, A. (1941). Solution of problems of elasticity by the framework method. *J.*
1389 *appl. Mech.*

1390 Hursan, G., & Zhdanov, M. S. (2002). Contraction integral equation method in three-
1391 dimensional electromagnetic modeling. *Radio Science*, 37(6), 1-1.

1392 Jaysaval, P., Shantsev, D., & de la Kethulle de Ryhove, S. (2014). Fast multimodel
1393 finite-difference controlled-source electromagnetic simulations based on a Schur
1394 complement approach. *Geophysics*, 79(6), E315-E327.

1395 Jaysaval, P., Shantsev, D. V., de la Kethulle de Ryhove, S., & Bratteland, T. (2016).
1396 Fully anisotropic 3-D EM modelling on a Lebedev grid with a multigrid
1397 pre-conditioner. *Geophysical Journal International*, 207(3), 1554-1572.

1398 Jin J. (2002). *The Finite Element Method in Electromagnetics*, 2nd edn. John Wiley &
1399 Sons, Inc.

1400 Kaikkonen, P. (1986). Numerical electromagnetic modeling including studies of
1401 characteristic dimensions: A review. *Surveys in Geophysics*, 8(3), 301-337.

1402 Kang, S., S. J. Seol, and J. Byun. (2012). A feasibility study of CO2 sequestration
1403 monitoring using the mCSEM method at a deep brine aquifer in a shallow sea:
1404 *Geophysics*, 77(2), E117-E126.

1405 Katz, D. S., Thiele, E. T., & Taflove, A. (1994). Validation and extension to three
1406 dimensions of the Berenger PML absorbing boundary condition for FD-TD
1407 meshes. *IEEE microwave and guided wave letters*, 4(8), 268-270.

1408 Kelbert, A., Meqbel, N., Egbert, G. D., & Tandon, K. (2014). ModEM: A modular
1409 system for inversion of electromagnetic geophysical data. *Computers &*
1410 *Geosciences*, 66, 40-53.

1411 Key, K., & Weiss, C. (2006). Adaptive finite-element modeling using unstructured
1412 grids: The 2D magnetotelluric example. *Geophysics*, 71(6), G291-G299.

1413 Key, K., & Owall, J. (2011). A parallel goal-oriented adaptive finite element method
1414 for 2.5-D electromagnetic modelling. *Geophysical Journal International*, 186(1),
1415 137-154.

1416 Key, K. (2016). MARE2DEM: a 2-D inversion code for controlled-source
1417 electromagnetic and magnetotelluric data. *Geophysical Journal International*,

1418 207(1), 571-588

1 1419 Khan, A., Ghorbanian, V., & Lowther, D. (2019). Deep Learning for magnetic field
2 estimation. *IEEE Transactions on Magnetism*, 55(6), 1-4.

3 1420
4 1421 Kong, F. N., S. E. Johnstad, T. Røsten, and H. Westerdahl. (2008). A 2.5d
5 finite-element-modeling difference method for marine CSEM modeling in
6 stratified anisotropic media: *Geophysics*, 73(1), F9-F19

7 1423
8 1424 Kordy, M., Wannamaker, P., Maris, V., Cherkaev, E., & Hill, G. (2016). 3-D
9 magnetotelluric inversion including topography using deformed hexahedral edge
10 finite elements and direct solvers parallelized on SMP computers—Part I: forward
11 problem and parameter Jacobians. *Geophysical Journal International*, 204(1),
12 74-93.

13 1428
14 1429 Kosloff, D. D., & Baysal, E. (1982). Forward modeling by a Fourier
15 method. *Geophysics*, 47(10), 1402-1412.

16 1430
17 1431 Kruglyakov, M., Geraskin, A., & Kuvshinov, A. (2016). Novel accurate and scalable
18 3-D MT forward solver based on a contracting integral equation method.
19 *Computers & geosciences*, 96, 208-217.

20 1433
21 1434 Kruglyakov, M., & Bloshanskaya, L. (2017). High-performance parallel solver for
22 integral equations of electromagnetics based on Galerkin method. *Mathematical
23 Geosciences*, 49(6), 751-776.

24 1436
25 1437 Kruglyakov, M., & Kuvshinov, A. (2018). Using high-order polynomial basis in 3-D
26 EM forward modeling based on volume integral equation method. *Geophysical
27 Journal International*, 213(2), 1387-1401.

28 1438
29 1439 Krylov, A. N. (1931). On the Numerical Solution of Equation by Which are
30 Determined in Technical Problems the Frequencies of Small Vibrations of
31 Material Systems. *Izvestiia Akademii nauk SSSR (in Russian)*. 7 (4): 491-539.

32 1441
33 1442 Kuzuoglu, M. & Mittra, R. (1996). Frequency dependence of the constitutive
34 parameters of causal perfectly matched anisotropic absorbers, *IEEE Microw.
35 Guid. Wave Lett.*, 6(12), 447-449.

36 1444
37 1445 Lebedev, V. I. (1964). Difference analogues of orthogonal decompositions, basic
38 differential operators and some boundary problems of mathematical physics. I.
39 *USSR Computational Mathematics and Mathematical Physics*, 4(3), 69-92.

40 1447
41 1448 LeCun, Y., Boser, B., Denker, J. S., Henderson, D., Howard, R. E., Hubbard, W., &
42 Jackel, L. D. (1989). Backpropagation applied to handwritten zip code
43 recognition. *Neural computation*, 1(4), 541-551.

44 1450
45 1451 LeCun, Y., Bengio, Y. & Hinton, G. (2015) Deep learning. *Nature* 521, 436-444.

46 1452
47 1453 Lee, K. H., and H. F. Morrison. (1985), A numerical solution for the electromagnetic
48 scattering by a two-dimensional inhomogeneity. *Geophysics*, 50, 1163-1165.

49 1454
50 1455 Li, G., Li, Y., Han, B., & Liu, Z. (2018). Application of the perfectly matched layer in
51 3-D marine controlled-source electromagnetic modelling. *Geophysical Journal
52 International*, 212(1), 333-344.

53 1457
54 1458 Li, J., Farquharson, C. G., & Hu, X. (2016). 3D vector finite-element electromagnetic
55 forward modeling for large loop sources using a total-field algorithm and
56 unstructured tetrahedral grids. *Geophysics*, 82(1), E1-E16.

57 1460
58 1461 Li, J., Liu, Y., Yin, C., Ren, X., & Su, Y. (2020). Fast imaging of time-domain
59
60
61
62
63
64
65

- 1462 airborne em data using deep learning technology. *Geophysics*, 1-38.
- 1 1463 Li, Y., & Key, K. (2007). 2D marine controlled-source electromagnetic modeling: Part
2
3 1464 1—An adaptive finite-element algorithm. *Geophysics*, 72(2), WA51-WA62.
- 4 1465 Li, Y., & Pek, J. (2008). Adaptive finite element modelling of two-dimensional
5 1466 magnetotelluric fields in general anisotropic media. *Geophysical Journal*
6 1467 *International*, 175(3), 942-954.
- 8 1468 Liu, C., Ren, Z., Tang, J., & Yan, Y. (2008). Three-dimensional magnetotellurics
9 1469 modeling using edgebased finite-element unstructured meshes. *Applied*
10 1470 *Geophysics*, 5(3), 170-180.
- 12 1471 Liu, R., Guo, R., Liu, J., Ma, C., & Guo, Z. (2018a). A hybrid solver based on the
13 1472 integral equation method and vector finite-element method for 3D
14 1473 controlled-source electromagnetic method modeling. *Geophysics*, 83(5),
16 1474 E319-E333.
- 18 1475 Liu, Y., Xu, Z., & Li, Y. (2018b). Adaptive finite element modelling of
19 1476 three-dimensional magnetotelluric fields in general anisotropic media. *Journal of*
20 1477 *Applied Geophysics*, 151, 113-124.
- 22 1478 Liu, Y., & Yin, C. (2014). 3D anisotropic modeling for airborne EM systems using
23 1479 finite-difference method. *Journal of Applied Geophysics*, 109, 186-194.
- 25 1480 Liu, Y., Yin, C., Qiu, C., Hui, Z., Zhang, B., Ren, X., & Weng, A. (2019). 3-D
26 1481 inversion of transient EM data with topography using unstructured tetrahedral
27 1482 grids. *Geophysical Journal International*, 217(1), 301-318.
- 29 1483 Maaø, F. A. (2007). Fast finite-difference time-domain modeling for
30 1484 marine-subsurface electromagnetic problems. *Geophysics*, 72(2), A19-A23.
- 32 1485 Mackie, R. L., Smith, J. T., & Madden, T. R. (1994). Three- dimensional
33 1486 electromagnetic modeling using finite difference equations: The magnetotelluric
34 1487 example. *Radio Science*, 29(4), 923-935.
- 36 1488 Maiti, S., and Tiwari, R. K. (2010). Automatic discriminations among geophysical
37 1489 signals via the Bayesian neural networks approach: *Geophysics*, 75, no.1,
38 1490 E67-E78.
- 40 1491 Manoj, C., and Nagarajan, N. (2003) The application of Artificial Neural Networks to
41 1492 magnetotelluric time-series analysis: *Geophysical Journal International*, 153,
42 1493 409-423.
- 44 1494 Miensopust, M. P., Queralt, P., Jones, A. G., & 3D MT modellers. (2013).
45 1495 Magnetotelluric 3-D inversion—A review of two successful workshops on
46 1496 forward and inversion code testing and comparison. *Geophysical Journal*
47 1497 *International*, 193(3), 1216-1238.
- 49 1498 Mitsuhashi, Y., 2000, 2-D electromagnetic modeling by finite-element method with a
50 1499 dipole source and topography: *Geophysics*, 65, 465-475.
- 52 1500 Mitsuhashi, Y., & Uchida, T. (2004). 3D magnetotelluric modeling using the T- Ω
53 1501 finite-element method. *Geophysics*, 69(1), 108-119.
- 55 1502 Mittet, R. (2010). High-order finite-difference simulations of marine CSEM surveys
56 1503 using a correspondence principle for wave and diffusion fields FDTD simulation
57 1504 of marine CSEM surveys. *Geophysics*, 75(1), F33-F50.
- 59 1505 Moghadas, D. (2020) One-dimensional deep learning inversion of electromagnetic
60
61
62
63
64
65

1 1506 induction data using convolutional neural network, *Geophysical Journal*
2 1507 *International*, 222(1):247-259.

3 1508 Mukherjee, S., & Everett, M. E. (2011). 3D controlled-source electromagnetic
4 1509 edge-based finite element modeling of conductive and permeable heterogeneities.
5 1510 *Geophysics*, 76(4), F215-F226.

6 1511 Mur, G. (1991). Finite- element modeling of three- dimensional electromagnetic
7 1512 fields in inhomogeneous media. *Radio Science*, 26(1), 275-280.

8 1513 Nam, M. J., Kim, H. J., Song, Y., Lee, T. J., Son, J. S., & Suh, J. H. (2007). 3D
9 1514 magnetotelluric modelling including surface topography. *Geophysical*
10 1515 *Prospecting*, 55(2), 277-287.

11 1516 Nédélec, J.C., 1980. Mixed finite elements in R^3 . *Numerische Mathematik*, 35,
12 1517 315-341.

13 1518 Newman, G. A., & Alumbaugh, D. L. (1995). Frequency-domain modelling of
14 1519 airborne electromagnetic responses using staggered finite differences.
15 1520 *Geophysical Prospecting*, 43(8), 1021-1042.

16 1521 Newman, G. A., & Alumbaugh, D. L. (2002). Three-dimensional induction logging
17 1522 problems, Part 2: A finite-difference solution. *Geophysics*, 67(2), 484-491.

18 1523 Newman, G. A. (2014). A review of high-performance computational strategies for
19 1524 modeling and imaging of electromagnetic induction data. *Surveys in*
20 1525 *Geophysics*, 35(1), 85-100.

21 1526 Noh, K., Yoon, D. & Byun, J. (2020) Imaging subsurface resistivity structure from
22 1527 airborne electromagnetic induction data using deep neural network, *Exploration*
23 1528 *Geophysics*, 51:2, 214-220.

24 1529 Oh, S., Noh, K., Yoon, D., Seol, S.J., & Byun, J. (2019). Salt delineation from
25 1530 electromagnetic data using convolutional neural networks. *IEEE Geoenvironment and*
26 1531 *Remote Sensing Letters*, 16(4), 519-523.

27 1532 Oristaglio, M. L., & Hohmann, G. W. (1984). Diffusion of electromagnetic fields into
28 1533 a two-dimensional earth: A finite-difference approach. *Geophysics*, 49(7),
29 1534 870-894.

30 1535 Owall, J.S., (2006). Asymptotically exact functional error estimators based on
31 1536 superconvergent gradient recovery, *Numer. Math.*, 102(3), 543-558.

32 1537 Pek, J., & Verner, T. (1997). Finite-difference modelling of magnetotelluric fields in
33 1538 two-dimensional anisotropic media. *Geophysical Journal International*, 128(3),
34 1539 505-521.

35 1540 Poulton, M., Sternberg, B. & Glass, C. (1992a). Neural network pattern recognition of
36 1541 subsurface EM images, *Journal of Applied Geophysics*, 29, 21-36.

37 1542 Poulton, M., Sternberg, B. & Glass, C. (1992b). Location of subsurface targets in
38 1543 geophysical data using neural networks, *Geophysics*, 57, 1534-1544.

39 1544 Poulton, M. & Birken, R.A. (1998). Estimating one-dimensional models from
40 1545 frequency-domain electromagnetic data using modular neural networks, *IEEE T*
41 1546 *rans. GeoScience and Remote Sensing*, 36, 547-559.

42 1547 Pridmore, D. F., Hohmann, G. W., Ward, S. H., & Sill, W. R. (1981). An investigation
43 1548 of finite-element modeling for electrical and electromagnetic data in three
44 1549 dimensions. *Geophysics*, 46(7), 1009-1024.

45
46
47
48
49
50
51
52
53
54
55
56
57
58
59
60
61
62
63
64
65

1 1550 Puzyrev, V., Koldan, J., de la Puente, J., Houzeaux, G., Vázquez, M., & Cela, J. M.
2 1551 (2013). A parallel finite-element method for three-dimensional controlled-source
3 1552 electromagnetic forward modelling. *Geophysical Journal International*, 193(2),
4 1553 678-693.
5 1554 Puzyrev, V., (2019). Deep learning electromagnetic inversion with convolutional
6 1555 neural networks. *Geophysical Journal International*, 218(2), 817-832.
7 1556 Quarteroni, A., Sacco, R., Saleri, F. (2010). *Numerical Mathematics*. vol. 37. Springer
8 1557 Science & Business Media.
9 1558 Ren, Z., & Tang, J. (2010). 3D direct current resistivity modeling with unstructured
10 1559 mesh by adaptive finite-element method. *Geophysics*, 75(1), H7-H17.
11 1560 Ren, Z., Kalscheuer, T., Greenhalgh, S., & Maurer, H. (2013). A goal-oriented
12 1561 adaptive finite-element approach for plane wave 3-D electromagnetic modelling.
13 1562 *Geophysical Journal International*, 194(2), 700-718.
14 1563 Ren, Z., Kalscheuer, T., Greenhalgh, S., & Maurer, H. (2014a). A finite-element-based
15 1564 domain-decomposition approach for plane wave 3D electromagnetic
16 1565 modeling. *Geophysics*, 79(6), E255-E268.
17 1566 Ren, Z., Kalscheuer, T., Greenhalgh, S., & Maurer, H. (2014b). A hybrid boundary
18 1567 element-finite element approach to modeling plane wave 3D electromagnetic
19 1568 induction responses in the Earth. *Journal of Computational Physics*, 258,
20 1569 705-717.
21 1570 Rijo, L. (1977). Modeling of electric and electromagnetic data.
22 1571 Rochlitz, R., Skibbe, N., & Günther, Thomas. (2018). custEM: customizable
23 1572 finite-element simulation of complex controlled-source electromagnetic data.
24 1573 *Geophysics*, 1-70.
25 1574 Rodi, W. L. (1976). A technique for improving the accuracy of finite element
26 1575 solutions for magnetotelluric data. *Geophysical Journal International*, 44(2),
27 1576 483-506.
28 1577 Saad, Y. (2003). *Iterative methods for sparse linear systems*: SIAM.
29 1578 SanFilipo, W. A., & Hohmann, G. W. (1985). Integral equation solution for the
30 1579 transient electromagnetic response of a three-dimensional body in a conductive
31 1580 half-space. *Geophysics*, 50(5), 798-809.
32 1581 Schenk, O., and Gärtner, K. (2004). Solving unsymmetric sparse systems of linear
33 1582 equations with PARDISO: *Future Generation Computer Systems*, 20, 475-487.
34 1583 Schwarzbach, C., Börner, R. U., Spitzer, K. (2011). Three-dimensional adaptive
35 1584 higher order finite element simulation for geo-electromagnetic: A marine CSEM
36 1585 example, *Geophysical Journal International*, 187, 63-74.
37 1586 Schwarzbach, C., Haber, E. (2013). Finite-element based inversion for time-harmonic
38 1587 electromagnetic problems. *Geophysical Journal International*, 193:615-634.
39 1588 Seiberl, W., Ahl, A. and Winkler, E. (1998). Interpretation of airborne electromagnetic
40 1589 data with neural networks: *Exploration Geophysics*, 29, 152-156.
41 1590 Shahriari, M., Pardo, D., Moser, B., Sobieczky, F. (2020). A Deep Neural Network as
42 1591 Surrogate Model for Forward Simulation of Borehole Resistivity Measurements.
43 1592 *Procedia Manufacturing* 42:235-238.
44 1593 Sheard, S. N., Ritchie, T. J., Christopherson, K. R., & Brand, E. (2005). Mining,
45
46
47
48
49
50
51
52
53
54
55
56
57
58
59
60
61
62
63
64
65

1 1594 environmental, petroleum, and engineering industry applications of
2 1595 electromagnetic techniques in geophysics. *Surveys in Geophysics*, 26(5),
3 1596 653-669.

4 1597 Siemon, B., Christiansen, A. V., & Auken, E. (2009). A review of helicopter- borne
5 1598 electromagnetic methods for groundwater exploration. *Near Surface Geophysics*,
6 1599 7(5-6), 629-646.

8 1600 Singer, B. S., & Fainberg, E. B. (1985). Electromagnetic induction in non-uniform
9 1601 thin layers. *Izmiran, Moscow*, 1(3), 5.

10 1602 Singer, B. S. (1995). Method for solution of Maxwell's equations in non-uniform
11 1603 media. *Geophysical Journal International*, 120(3), 590-598.

12 1604 Singer, B. S. (2008). Electromagnetic integral equation approach based on contraction
13 1605 operator and solution optimization in Krylov subspace. *Geophysical Journal*
14 1606 *International*, 175(3), 857-884.

15 1607 Smith, J. T. (1996a). Conservative modeling of 3-D electromagnetic fields, Part I:
16 1608 Properties and error analysis. *Geophysics*, 61(5), 1308-1318.

17 1609 Smith, J. T. (1996b). Conservative modeling of 3-D electromagnetic fields, Part II:
18 1610 Biconjugate gradient solution and an accelerator. *Geophysics*, 61(5), 1319-1324.

19 1611 Spichak, V., Popova, I. (2000) Artificial neural network inversion of magnetotelluric
20 1612 data in terms of three-dimensional earth macroparameters, *Geophysical Journal*
21 1613 *International*, 142(1), 15-26.

22 1614 Stoyer, C. H., and R. J. Greenfield. (1976). Numerical solutions of the response of a
23 1615 two-dimensional earth to an oscillating magnetic dipole source: *Geophysics*, 41,
24 1616 519-530.

25 1617 Strack, K. M. (2014). Future directions of electromagnetic methods for hydrocarbon
26 1618 applications. *Surveys in Geophysics*, 35(1), 157-177.

27 1619 Streich, R. (2009). 3D finite-difference frequency-domain modeling of
28 1620 controlled-source electromagnetic data: Direct solution and optimization for high
29 1621 accuracy. *Geophysics*, 74(5), F95-F105.

30 1622 Streich, R. (2016). Controlled-source electromagnetic approaches for hydrocarbon
31 1623 exploration and monitoring on land. *Surveys in Geophysics*, 37(1), 47-80.

32 1624 Sugeng, F. (1998). Modeling the 3D TDEM response using the 3D full-domain
33 1625 finite-element method based on the hexahedral edge-element technique.
34 1626 *Exploration Geophysics*, 29(4), 615-619.

35 1627 Sun, J., & Kuvshinov, A. (2014). Accelerating EM integral equation forward solver
36 1628 for global geomagnetic induction using SVD based matrix compression method.
37 1629 *Geophysical Journal International*, 200(2), 1005-1011.

38 1630 Tang, W., Shan, T., Dang, X., Li, M., Yang, F., Xu, S., & Wu, J. (2017). Study on a
39 1631 Poisson's equation solver based on deep learning technique. *IEEE Electrical*
40 1632 *Design of Advanced Packaging and Systems Symposium (EDAPS)* , 1-3.

41 1633 Ting, S. C., & Hohmann, G. W. (1981). Integral equation modeling of
42 1634 three-dimensional magnetotelluric response. *Geophysics*, 46(2), 182-197.

43 1635 Um, E. S., Harris, J. M., & Alumbaugh, D. L. (2010). 3D time-domain simulation of
44 1636 electromagnetic diffusion phenomena: A finite-element electric-field
45 1637 approachFinite-element time-domain simulation. *Geophysics*, 75(4), F115-F126.

46
47
48
49
50
51
52
53
54
55
56
57
58
59
60
61
62
63
64
65

1 1638 Um, E. S., Harris, J. M., & Alumbaugh, D. L. (2012). An iterative finite element
2 1639 time-domain method for simulating three-dimensional electromagnetic diffusion
3 1640 in earth. *Geophysical Journal International*, 190(2), 871-886.

4 1641 Unsworth, M. J., Travis, B. J., and Chave, A. D. (1993). Electromagnetic induction by
5 1642 a finite electric dipole source over a 2-D earth: *Geophysics*, 58, 198-214.

6 1643 Varilsuha, D., & Candansayar, M. E. (2018). 3D magnetotelluric modeling by using
7 1644 finite-difference method: Comparison study of different forward modeling
8 1645 approaches. *Geophysics*, 83(2), WB51-WB60.

9 1646 Virieux, J., Calandra, H., & Plessix, R. E. (2011). A review of the spectral,
10 1647 pseudo-spectral, finite-difference and finite-element modelling techniques for
11 1648 geophysical imaging. *Geophysical Prospecting*, 59(5), 794-813.

12 1649 Wait, J. R. (1962). *Electromagnetic waves in stratified media*: New York, MacMillan.

13 1650 Walker, P. W., & West, G. F. (1991). A robust integral equation solution for
14 1651 electromagnetic scattering by a thin plate in conductive media. *Geophysics*,
15 1652 56(8), 1140-1152.

16 1653 Wang, T., & Hohmann, G. W. (1993). A finite-difference, time-domain solution for
17 1654 three-dimensional electromagnetic modeling. *Geophysics*, 58(6), 797-809.

18 1655 Wang, T., & Fang, S. (2001). 3-D electromagnetic anisotropy modeling using finite
19 1656 differences. *Geophysics*, 66(5), 1386-1398.

20 1657 Wannamaker, P. E., Hohmann, G. W., & SanFilipo, W. A. (1984). Electromagnetic
21 1658 modeling of three-dimensional bodies in layered earths using integral equations.
22 1659 *Geophysics*, 49(1), 60-74.

23 1660 Wannamaker, P. E., Stodt, J. A., & Rijo, L. (1986). Two-dimensional topographic
24 1661 responses in magnetotellurics modeled using finite elements. *Geophysics*, 51(11),
25 1662 2131-2144.

26 1663 Wannamaker, P. E., Stodt, J. A., & Rijo, L. (1987). A stable finite-element solution for
27 1664 two-dimensional magnetotelluric modeling: *Geophysical Journal of the Royal
28 1665 Astronomical Society*, 88, 277-296.

29 1666 Wannamaker, P. E. (1991). Advances in three-dimensional magnetotelluric modeling
30 1667 using integral equations. *Geophysics*, 56(11), 1716-1728.

31 1668 Weiss, C. J., & Newman, G. A. (2002). Electromagnetic induction in a fully 3-D
32 1669 anisotropic earth. *Geophysics*, 67(4), 1104-1114.

33 1670 Wu, X., Xue, G., He, Y., & Xue, J. (2020). Removal of the multi-source noise in
34 1671 airborne electromagnetic data based on deep learning. *Geophysics*, 1-72.

35 1672 Xiong, Z. (1992). Electromagnetic modeling of 3-D structures by the method of
36 1673 system iteration using integral equations. *Geophysics*, 57(12), 1556-1561.

37 1674 Xiong, Z., & Tripp, A. C. (1993). Scattering matrix evaluation using spatial symmetry
38 1675 in electromagnetic modelling. *Geophysical Journal International*, 114(3),
39 1676 459-464.

40 1677 Yavich, N., & Zhdanov, M. S. (2016). Contraction pre-conditioner in finite-difference
41 1678 electromagnetic modelling. *Geophysical Journal International*, 206(3),
42 1679 1718-1729.

43 1680 Yee, K. (1966). Numerical solution of initial boundary value problems involving
44 1681 Maxwell's equations in isotropic media. *IEEE Transactions on antennas and*

45
46
47
48
49
50
51
52
53
54
55
56
57
58
59
60
61
62
63
64
65

1682 propagation, 14(3), 302-307.

1 1683 Yin, C., Zhang, B. Liu, Y. and Cai, J. (2016). A goal-oriented adaptive finite element
2
3 1684 method for 3D scattered airborne electromagnetic method modeling: *Geophysics*,
4 1685 81(5), E337-E346.

5 1686 Yoon, D., Zhdanov, M. S., Mattsson, J., Cai, H., & Gribenko, A. (2016). A hybrid
6
7 1687 finite-difference and integral-equation method for modeling and inversion of
8 1688 marine controlled-source electromagnetic data. *Geophysics*, 81(5), E323-E336.

9 1689 Yoshimura, R., & Oshiman, N. (2002). Edge- based finite element approach to the
10
11 1690 simulation of geoelectromagnetic induction in a 3- D sphere. *Geophysical*
12
13 1691 *Research Letters*, 29(3).

14 1692 Zaslavsky, M., Druskin, V., Davydycheva, S., Knizhnerman, L., Abubakar, A., &
15 1693 Habashy, T. (2011). Hybrid finite-difference integral equation solver for 3D
16 1694 frequency domain anisotropic electromagnetic problems. *Geophysics*, 76(2),
17 1695 F123-F137.

18 1696 Zeng, S., Chen, F., Li, D., Chen, J., & Chen, J. (2018). A novel 2.5 D finite difference
19
20 1697 scheme for simulations of resistivity logging in anisotropic media. *Journal of*
21
22 1698 *Applied Geophysics*, 150, 144-152.

23 1699 Zhang, J., Mackie, R. L., & Madden, T. R. (1995). 3-D resistivity forward modeling
24
25 1700 and inversion using conjugate gradients. *Geophysics*, 60(5), 1313-1325.

26 1701 Zhang, B., Yin, C., Ren, X., Liu, Y., & Qi, Y. (2018). Adaptive finite element for 3D
27
28 1702 time-domain airborne electromagnetic modeling based on hybrid posterior error
29
30 1703 estimation. *Geophysics*, 83(2), WB71-WB79.

31 1704 Zhang, Y., and Paulson, K. V. (1997). Magnetotelluric inversion using regularized
32
33 1705 Hopfield neural networks: *Geophysical Prospecting*, 45, 725-743.

34 1706 Zhang, L., Poulton, M. M. and Wang, T. (2002) Borehole electrical resistivity
35
36 1707 modeling using neural networks: *Geophysics*, 67, 1790-1797.

37 1708 Zhdanov, M. S. (2010). *Electromagnetic geophysics: Notes from the past and the road*
38
39 1709 *ahead. Geophysics*, 75(5), 75A49-75A66.

40 1710 Zhdanov, M. S., Dmitriev, V. I., Fang, S., & Hursán, G. (2000). Quasi-analytical
41
42 1711 approximations and series in electromagnetic modeling. *Geophysics*, 65(6),
43
44 1712 1746-1757.

45 1713 Zhdanov, M. S., & Fang, S. (1996). Quasi-linear approximation in 3-D
46
47 1714 electromagnetic modeling. *Geophysics*, 61(3), 646-665.

48 1715 Zhdanov, M. S., Lee, S. K., & Yoshioka, K. (2006). Integral equation method for 3D
49
50 1716 modeling of electromagnetic fields in complex structures with inhomogeneous
51
52 1717 background conductivity. *Geophysics*, 71(6), G333-G345.

53 1718 Zyserman, F. I., & Santos, J. E. (2000). Parallel finite element algorithm with domain
54
55 1719 decomposition for three-dimensional magnetotelluric modelling. *Journal of*
56
57 1720 *Applied Geophysics*, 44(4), 337-351.

58
59
60
61
62
63
64
65